

Eddy-Mediated Mixing of Oxygen in the Equatorial Pacific

Yassir A. Eddebbar¹, Daniel Bridger Whitt², Ariane Verdy³, Matthew R. Mazloff³, Aneesh Subramanian⁴, and Matthew C. Long⁵

¹Scripps Institution of Oceanography, University of California San Diego

²NASA Ames Research Center

³UCSD

⁴University of Colorado

⁵National Center for Atmospheric Research (UCAR)

September 30, 2023

Abstract

In the tropical Pacific, weak ventilation and intense microbial respiration at depth give rise to a low dissolved oxygen (O₂) environment that is thought to be ventilated primarily by the equatorial current system (ECS). The role of mesoscale eddies and diapycnal mixing as potential pathways of O₂ supply in this region, however, remains poorly known due to sparse observations and coarse model resolution. Using an eddy resolving simulation of ocean circulation and biogeochemistry, we assess the contribution of these processes to the O₂ budget balance and find that turbulent mixing of O₂ and its modulation by mesoscale eddies contribute substantially to the replenishment of O₂ in the upper equatorial Pacific thermocline, complementing the advective supply of O₂ by the ECS and meridional circulation at depth. These transport processes are strongly sensitive to seasonal forcing by the wind, with elevated mixing of O₂ into the upper thermocline during summer and fall when the vertical shear of the lateral flow and eddy kinetic energy are intensified. The tight link between eddy activity and the downward mixing of O₂ arises from the modulation of equatorial turbulence by Tropical Instability Waves via their eddy impacts on the vertical shear. This interaction of ocean processes across scales sustains a local pathway of O₂ delivery into the equatorial Pacific interior and highlights the need for adequate observations and model representation of turbulent mixing and mesoscale processes for understanding and predicting the fate of the tropical Pacific O₂ content in a warmer and more stratified ocean.

Eddy-Mediated Mixing of Oxygen in the Equatorial Pacific

Yassir A. Eddebbar¹, Daniel B. Whitt², Ariane Verdy¹, Matthew R. Mazloff¹,
Aneesh C. Subramanian³, Matthew C. Long⁴

¹Scripps Institution of Oceanography, University of California San Diego, La Jolla, CA

²Ames Research Center, NASA, Moffett Field, CA

³Atmospheric and Oceanic Sciences, Colorado University, Boulder, CO

⁴National Center for Atmospheric Research, Boulder, CO

Key Points:

- Vertical mixing is an important source of oxygen supply to the upper equatorial Pacific thermocline.
- The simulated supply of oxygen by advection and vertical mixing is strongly seasonal and is driven by seasonal variability in the wind.
- The vertical mixing of oxygen is strongly modulated by the simulated mesoscale eddy impacts on equatorial shear-driven turbulence.

Corresponding author: Yassir Eddebbar, yeddebba@ucsd.edu

Abstract

In the tropical Pacific, weak ventilation and intense microbial respiration at depth give rise to a low dissolved oxygen (O_2) environment that is thought to be ventilated primarily by the equatorial current system (ECS). The role of mesoscale eddies and diapycnal mixing as potential pathways of O_2 supply in this region, however, remains poorly known due to sparse observations and coarse model resolution. Using an eddy resolving simulation of ocean circulation and biogeochemistry, we assess the contribution of these processes to the O_2 budget balance and find that turbulent mixing of O_2 and its modulation by mesoscale eddies contribute substantially to the replenishment of O_2 in the upper equatorial Pacific thermocline, complementing the advective supply of O_2 by the ECS and meridional circulation at depth. These transport processes are strongly sensitive to seasonal forcing by the wind, with elevated mixing of O_2 into the upper thermocline during summer and fall when the vertical shear of the lateral flow and eddy kinetic energy are intensified. The tight link between eddy activity and the downward mixing of O_2 arises from the modulation of equatorial turbulence by Tropical Instability Waves via their eddy impacts on the vertical shear. This interaction of ocean processes across scales sustains a local pathway of O_2 delivery into the equatorial Pacific interior and highlights the need for adequate observations and model representation of turbulent mixing and mesoscale processes for understanding and predicting the fate of the tropical Pacific O_2 content in a warmer and more stratified ocean.

Plain Language Summary

The eastern tropical Pacific interior is an O_2 deficient environment, due to intense O_2 consumption by microbial communities that is not vigorously replenished by ocean circulation at depth. In this study, we use a high resolution simulation of ocean circulation and biogeochemistry to understand the role of finer scale processes such as turbulence and eddies in injecting O_2 locally. We find that mixing due to turbulence along the equator supplies a key portion of O_2 into the ocean by exchanging waters between the well-aerated mixed layer near the surface and the ocean's interior where O_2 falls precipitously with depth. We also find that this mixing varies considerably with the seasons. This annual cycle in mixing arises from the seasonal passage of eddies, which amplifies turbulence through their influence on the subsurface currents along the equator, and represents a previously unexplored but potentially important route of O_2 delivery into the ocean's interior. As the upper ocean warms and becomes less dense, the ocean's O_2 content is expected to decrease, and thus observing and accurately modeling these O_2 pathways will be crucial to monitoring how marine ecosystem habitats will shift in a warmer climate.

1 Introduction

Aerobic marine organisms in the tropical Pacific navigate a complex habitat, set by high productivity in the euphotic layer along the upwelling regions and scarce dissolved oxygen (O_2) at depth. This O_2 scarcity is set by a net balance of weak O_2 supply and intense microbial consumption in the thermocline (Sverdrup, 1938; Wyrski, 1962; Karstensen et al., 2008), giving rise to large O_2 deficient zones (ODZs) at depth where O_2 levels fall below hypoxic thresholds (Gray et al., 2002; Vaquer-Sunyer & Duarte, 2008). These ODZs have exhibited a concerning expansion in recent decades, threatening to further compress the ecosystem habitats and foraging range of pelagic fisheries (Stramma et al., 2012; Gallo & Levin, 2016). Though O_2 decline at high and mid-latitudes is expected due to the sensitivity of O_2 solubility and ocean ventilation to warming (Keeling et al., 2010), a mechanistic explanation for the observed tropical Pacific O_2 loss is lacking due to poor understanding of the processes governing O_2 supply and its variability in this region (Brandt et al., 2015; Oschlies et al., 2018). This is especially evident in the equatorial Pacific which accounts for the largest reported O_2 loss globally in recent decades (Schmidtke et al., 2017) and where the energetic circulation (Figure 1) exerts a complex and poorly understood influence on O_2 structure and variability (Stramma et al., 2010; Margolskee et al., 2019; Busecke et al., 2019).

The reported O_2 decline in the equatorial Pacific of 210 ± 125 Tmol per decade since 1960 (Schmidtke et al., 2017) has coincided with a multidecadal strengthening of the Equatorial Undercurrent (EUC) (Drenkard & Karneuskas, 2014). This is puzzling given the EUC's role as the main pathway of O_2 supply to the central and eastern equatorial Pacific (Stramma et al., 2010; Busecke et al., 2019): an intensification of the EUC would be expected to increase O_2 levels in the eastern and central equatorial Pacific, as analogously shown by the strengthening of the Atlantic EUC and its subsequent oxygenation of the upper equatorial Atlantic (Brandt et al., 2021). The EUC, however, is also a major source of nutrients to the eastern and central equatorial Pacific (Ryan et al., 2006), which can indirectly influence O_2 levels by fueling productivity at the surface and intensifying consumption at depth. O_2 is also supplied via the north and south subsurface counter-currents ("Tsuchiya" jets) and the intermediate counter-currents, and though their volume transport is much weaker than the EUC, these jets represent important ventilation pathways due to their deeper isopycnal range and their off-equator deflection into the ODZ regions (Stramma et al., 2010; Margolskee et al., 2019).

A potentially important but less explored pathway of O_2 supply in the equatorial Pacific concerns the transport by mesoscale eddies, which exhibit pronounced and regionally distinct imprints on O_2 distribution and variability in ocean models (Bettencourt et al., 2015; Frenger et al., 2018; Eddebbar et al., 2021). Tropical instability vortices (TIVs), which are large and fast propagating eddies that are associated with Tropical Instability Waves (TIWs), strongly influence the instantaneous O_2 distribution during their westward propagation (Eddebbar et al., 2021) due to their intense vertical and lateral circulation (Kennan & Flament, 2000). The net effect of eddy transport on O_2 supply and its steady state and seasonal budget balance in the equatorial Pacific, however, have so far not been quantified, and its representation in climate models may contribute to their O_2 biases which persist across model generations (Cabr   et al., 2015; Busecke et al., 2019, 2022). And while diffusive mixing has been recently proposed as a potential source of O_2 at depth in the Atlantic basin (Hahn et al., 2014; Brandt et al., 2015; Calil, 2023) and a key factor for future O_2 projections (Couespel et al., 2019; Portela et al., 2020; L  vy et al., 2022), its net contribution to the O_2 budget and the processes underlying its spatial and temporal variability are poorly known. This is especially of interest in the equatorial Pacific, where the thermocline is shallow and where the high shear (Figure 1d) induced by the EUC and South Equatorial Current (SEC) induces intense turbulent mixing and substantial heat exchange between the thermocline and the surface layer (Moum et al., 2009; Holmes & Thomas, 2015; Cherian et al., 2021; Whitt et al., 2022).

These advective and mixing processes governing O_2 transport in the equatorial Pacific are tightly intertwined across temporal and spatial scales. Shear-driven turbulence along the equatorial cold tongue, for instance, is seasonally modulated by the propagation of TIWs and their eddy structures (Moum et al., 2013; Lien et al., 2008; Holmes & Thomas, 2015; Cherian et al., 2021), which themselves arise from barotropic and baroclinic instabilities generated by the shear between the zonal jets (Willett et al., 2006). These physical interactions may also play key roles in facilitating the vertical supply of nutrients from the EUC to the euphotic layer along the equatorial Pacific, intensifying productivity at the surface (Strutton et al., 2001; Vichi et al., 2008; Strutton et al., 2011; Tian et al., 2018), and potentially modulating O_2 consumption rates in the thermocline. Identifying the contributions and mechanisms by which these transport processes balance O_2 removal in the ocean interior is critical for understanding the observed expansion of the ODZs and predicting their future (Busecke et al., 2022), but has so far been hindered by sparse sampling (Brandt et al., 2015; Ito et al., 2017) and inadequate representation of the equatorial current system and mesoscale eddies in coarse models (Cabré et al., 2015; Busecke et al., 2019).

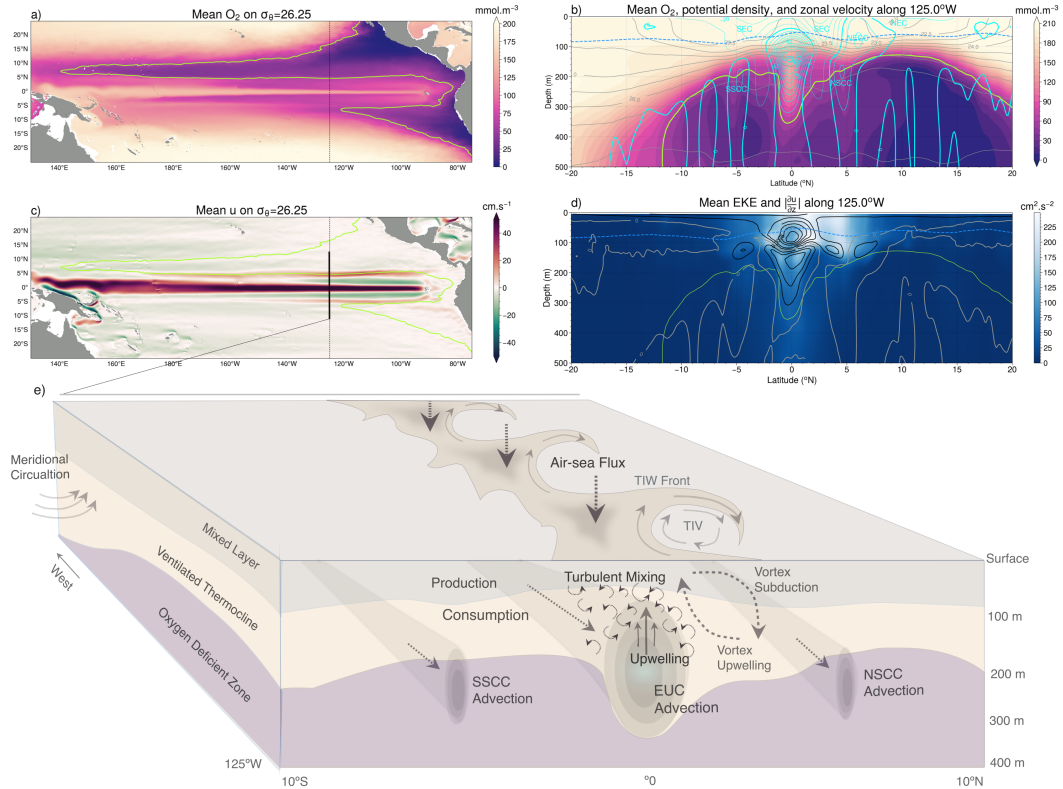


Figure 1. Tropical Pacific O_2 distribution and driving processes. Mean O_2 on the 26.25 isopycnal (a) and along $125^\circ W$ (b) with zonal velocity (cyan) contoured every 10 cm.s^{-1} (bold denotes zero, dashed indicate negative values), potential density (gray), mixed layer depth (dashed blue), and hypoxic boundary (lime) in the CESM simulation. c) Mean eastward zonal velocity on the 26.25 isopycnal. d) Mean eddy kinetic energy (EKE) in shading and the absolute mean vertical shear of the zonal velocity ($|\frac{\partial u}{\partial z}|$) contoured every 0.0025 s^{-1} (gray denotes zero) along $125^\circ W$. The mixed layer depth (dashed blue line) is defined using the maximum buoyancy gradient criteria of Large et al. (1997). e) Key processes driving O_2 supply and removal in the equatorial Pacific.

Here, we evaluate the contribution of advective and mixing processes in the equatorial Pacific O_2 budget balance and its seasonality using an eddy resolving simulation of ocean circulation and biogeochemistry. We focus our regional analysis on key processes governing O_2 supply into the upper (0-300 m) eastern and central equatorial Pacific (east of $160^\circ W$ and equatorward of $7^\circ S$ and $7^\circ N$), a highly energetic region that is thought to be ventilated primarily by the EUC and Tsuchiya jets (Stramma et al., 2010). Given their relatively well studied impacts on the transport of heat in the upper equatorial Pacific, we expect that eddy circulation and turbulent mixing may play similarly critical roles in the supply of O_2 in this region. Section 2 details our modeling and budget analysis framework. Next, we assess the steady state O_2 budget and seasonal variability of O_2 supply in the upper equatorial Pacific in Section 3 and Section 4, respectively. We conclude with an exploration of the mechanisms underlying the eddy-mediated mixing of O_2 in the upper equatorial Pacific thermocline in Section 5, followed by a summary and discussion of our findings in Section 6.

2 Methods

2.1 Ocean Model

We evaluate the contribution of physical and biogeochemical drivers of the mean and seasonal O_2 budget balance and their underlying processes using a 5-year eddy resolving hindcast simulation of the Community Earth System Model (CESM) version 1. In this configuration, the ocean is simulated using the Parallel Ocean Program version 2 (POP2) (Smith et al., 2010) with a grid resolution decreasing from 11 km near the equator to 3 km near the poles, and a vertical resolution increasing across 62 layers from 10 m in the upper 160 m to 250m in the abyss. Mixing is parameterized using the K-profile parameterization (KPP) framework, which represents shear-driven turbulent diffusion via a non-linear function of the local gradient Richardson number (Large et al., 1994). Ocean biogeochemistry is simulated using the Biogeochemical Elemental Cycle (BEC) model (Moore et al., 2013), which simulates lower trophic plankton dynamics, including three phytoplankton functional groups and one zooplankton group, coupled to the biogeochemical cycles of oxygen, carbon, and nutrients (Long et al., 2013).

The hindcast simulation of CESM is forced with a repeating annual climatological cycle of the atmospheric state using the Coordinated Ocean-Ice Reference Experiment (CORE) framework (Large & Yeager, 2004; Griffies et al., 2009). Ocean physical and biogeochemical properties were initialized using interpolated climatological fields from mapped observational products when available, e.g. the World Ocean Circulation Experiment (Gouretski & Koltermann, 2004) for temperature and salinity, and the World Ocean Atlas (WOA) for O_2 and macro-nutrients (Garcia et al., 2005), and when not available using interpolated fields from a previous hindcast CESM simulation integrated at the nominal 1° resolution (Long et al., 2013). The model was spun up for 15 years for physics and one year for biogeochemistry (Harrison et al., 2018), and then integrated forward for 5 years using the CORE atmospheric climatological annual cycle, and outputs were saved at 5 day frequencies. Despite its short duration, this spin up period allows the mesoscale circulation and its imprints on biogeochemical and plankton distributions to develop and stabilize enough while operating on tracer distributions that are similar to the mapped observational products used for initialization (e.g. O_2 and macro-nutrients), and has been recently used to evaluate the impact of eddies across a range of ocean biogeochemical cycles (Harrison et al., 2018; Song et al., 2018; Rohr et al., 2020; Eddebbar et al., 2021).

At the 0.1° resolution, CESM yields an energetic mesoscale eddy field with more realistic winter mixed layers and chlorophyll distributions than the more widely used 1° configuration (Harrison et al., 2018; Rohr et al., 2020), and generally reproduces the broad scale distribution of the eddy-induced correlation between chlorophyll and sea surface

height anomalies observed from satellites (Song et al., 2018). In the equatorial Pacific, ocean circulation and O_2 structure are generally improved at 0.1° vs the 1° solution, with strong seasonality in the zonal flow and meridional shear that gives rise to well resolved TIWs and their chlorophyll imprints (Eddebbar et al., 2021). The 0.1° configuration is also characterized by a less zonally tilted EUC and the emergence of the Tsuchiya jets and yields more realistic O_2 distributions (Eddebbar et al., 2021), in general agreement with recent global and regional model simulations that showcase improved representation of tropical Pacific ocean circulation and O_2 structures at higher resolution (Busecke et al., 2019; Margolskee et al., 2019).

2.2 Oxygen Budget

We assess the contribution of different processes to the O_2 budget balance, calculated in CESM as follow:

$$\frac{\partial O_2}{\partial t} = -\nabla \cdot (\mathbf{u}O_2) + D(O_2) + \frac{\partial}{\partial z} k \frac{\partial O_2}{\partial z} + J(O_2) \quad (1)$$

where $-\nabla \cdot (\mathbf{u}O_2)$ represents the lateral and vertical O_2 advection, $D(O_2)$ and $\frac{\partial}{\partial z} k \frac{\partial O_2}{\partial z}$ represent lateral and vertical diffusive mixing, respectively, and $J(O_2)$ represents the net balance between production of O_2 via photosynthesis and consumption by microbial respiration.

We assess the contribution of different budget terms in steady state by decomposing the advection term into a mean and eddy advective component using a Reynolds decomposition (McGillicuddy Jr et al., 2003) in the time-averaged budget equation as follow:

$$\overline{\frac{\partial O_2}{\partial t}} = -\nabla \cdot (\overline{\mathbf{u}}\overline{O_2}) - \nabla \cdot (\overline{\mathbf{u}'O_2'}) + \overline{D(O_2)} + \overline{\frac{\partial}{\partial z} k \frac{\partial O_2}{\partial z}} + \overline{J(O_2)} \quad (2)$$

where the bar denotes the average of the climatological monthly mean over the 5 year model solution, $-\nabla \cdot (\overline{\mathbf{u}}\overline{O_2})$ represents lateral and vertical O_2 advection by the mean flow, $-\nabla \cdot (\overline{\mathbf{u}'O_2'})$ quantifies the eddy advection effects, $\overline{\frac{\partial}{\partial z} k \frac{\partial O_2}{\partial z}}$ represents the mean contribution of vertical diffusive mixing, and $\overline{J(O_2)}$ represents the balance of mean O_2 production and consumption by photosynthesis and microbial consumption.

The eddy term $(-\nabla \cdot (\overline{\mathbf{u}'O_2'}))$, which quantifies the covariance of the time-deviating anomalies in the O_2 advection divergence, is calculated as the difference of the total and mean advective terms as:

$$-\nabla \cdot (\overline{\mathbf{u}'O_2'}) = -\nabla \cdot (\overline{\mathbf{u}O_2}) + \nabla \cdot (\overline{\mathbf{u}}\overline{O_2}) \quad (3)$$

Our choice of using the 5-day mean deviations from the 5-year climatological monthly mean for the eddy term in the Reynolds decomposition aims at isolating the effects of eddy advection from the large scale mean advective processes (e.g. ECS) as well as their seasonal variability.

The effects of mesoscale eddy lateral mixing is explicitly resolved at this resolution and the parameterized lateral diffusive mixing ($\overline{D(O_2)}$) is negligible compared to other budget terms and is not shown here for brevity. Our analysis of the seasonal cycle in Section 4 is based on seasonally averaging the climatological monthly means for boreal winter using December through February, boreal spring using March through May, boreal summer using June through August, and boreal fall using September through November.

3 The Oxygen Budget Balance in Steady State

We first consider the contribution of different physical and biogeochemical processes to the steady state budget balance and structure of O_2 , shown in Figure 2 as zonal averages over the eastern and central equatorial Pacific (80°W - 160°W). This region is characterized by enriched O_2 values in the mixed layer due to intense air-sea gas exchange and photosynthetic production of O_2 , overlaying a shallow oxycline that bounds the northern and southern tropical Pacific ODZs (Figure 2a). This complex subsurface structure is set by a net balance of large and often opposing contributions from transport and biological processes (Figure 2 and Figure S1 in Supporting Information). Microbial consumption is a major sink of O_2 throughout the equatorial Pacific thermocline, with intensified consumption centered around 5°S and 5°N , reflecting the divergence of sinking organic carbon away from its equatorial source of production via Ekman divergence and the tropical cells (Figure 2d). This O_2 removal is largely replenished by vigorous vertical mixing in the upper thermocline (50 – 150 m, $23.5 < \sigma_\theta < 25.5$ kg m^{-3}), though advection plays a more dominant role in supplying O_2 deeper in the thermocline (> 150 m, $\sigma_\theta > 25.5$ kg m^{-3}) and particularly near the ODZ boundaries (Figure 2b).

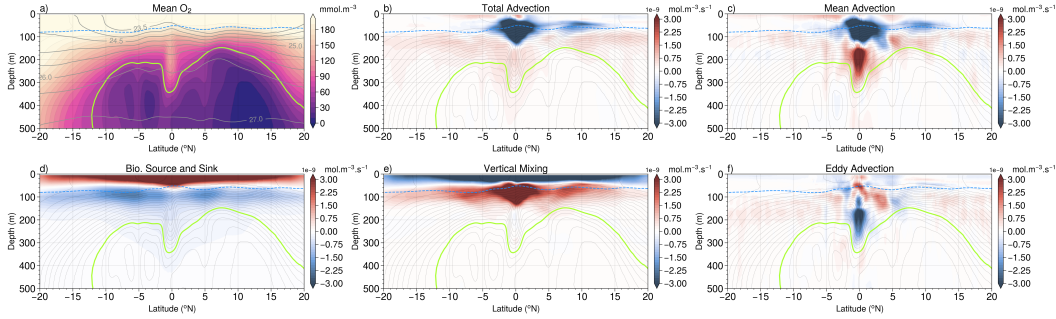


Figure 2. Mean O_2 budget decomposition zonally averaged over the eastern and central equatorial Pacific (80°W - 160°W) in the upper 500 m in CESM, including a) mean O_2 concentrations and potential density (gray contours), and contributions of b) total advection, c) mean advection, d) biological sources and sinks, e) vertical mixing, and f) eddy advection to the steady state O_2 budget balance. Positive values in b-f) denote positive contribution to the O_2 budget balance. Dashed blue line outline the mixed layer depth, grey contours in b-f) outline mean O_2 concentrations contoured every 10 mmol.m^{-3} , and the hypoxic boundary is shown in neon.

The contribution of advection shown in Figure 2b reflects both i) a “mean” component associated with large scale upwelling and lateral flow by the ECS and the shallow overturning circulation, and ii) an “eddy” component associated with the westward propagation of TIWs and their vortex structures (i.e. TIVs) which dominate eddy kinetic energy (EKE) in this region (Ubelmann & Fu, 2011), as well as meanderings and instabilities generated along the EUC path at depth. A decomposition of these mean and eddy terms (Figure 2b-c and 2f) shows that mean advection acts both to i) substantially reduce O_2 levels below and within the surface mixed layer between 2°S and 5°N via the large scale upwelling of low- O_2 thermocline waters to the surface (Figure S1f and S1i in Supporting Information), and ii) supply O_2 to the eastern basin west of 160°W through the zonal and meridional flow of waters (Figure S1d-e and S1g-h in Supporting Information). The lateral supply of O_2 from the western part of the equatorial Pacific basin to the east is driven largely by the EUC, which transports about 4.66×10^6 mol s^{-1} of oxygen across 160°W from the base of the mixed layer through $\sigma_\theta=26.5$ kg m^{-3} . This zonal EUC transport is further supplemented poleward of 4°N and 4°S by the Tsuchiya Jets which together advect about 0.41×10^6 mol s^{-1} of oxygen across 160°W , and the

convergence of ventilated waters by the tropical and subtropical cells which advect a net equatorward flux of $1.95 \times 10^6 \text{ mol s}^{-1}$ of oxygen across 7°S and 7°N from the base of the mixed layer through $\sigma_\theta = 26.5 \text{ kg m}^{-3}$ (Figure S1d-e and S1g-h in Supporting Information).

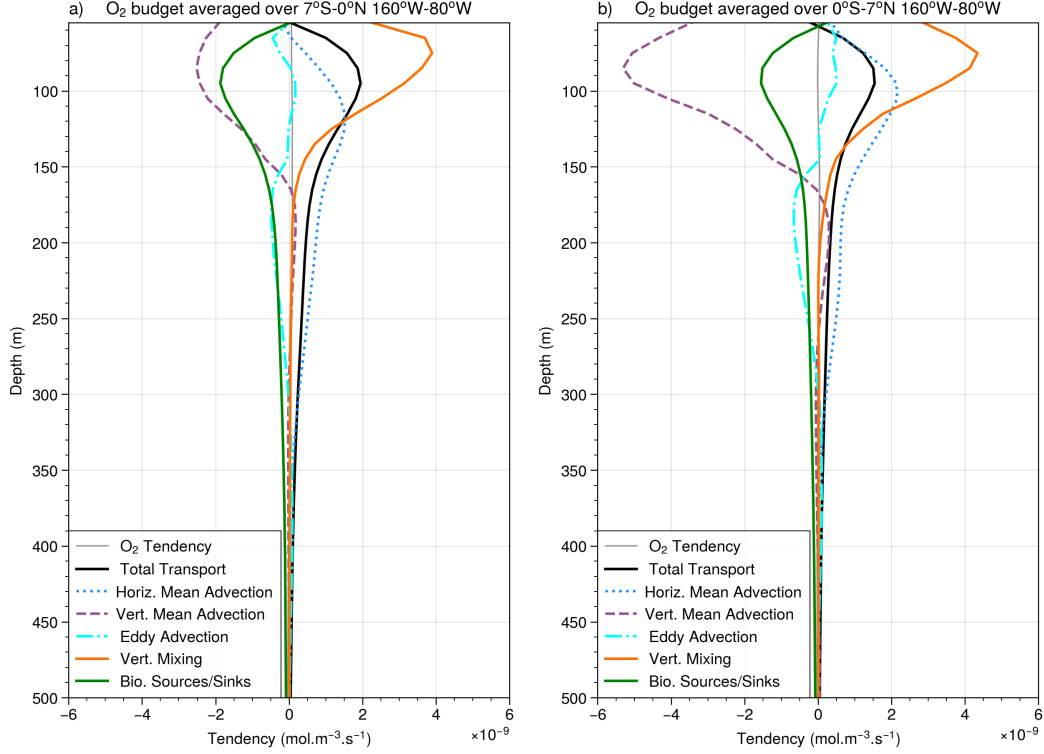


Figure 3. Mean O_2 budget decomposition laterally averaged over a) the southern (7°S - 0°) and b) northern (0° - 7°N) central and eastern (80°W - 160°W) equatorial Pacific in CESM. Total transport (black line) includes contributions from mean and eddy advection as well as vertical mixing, while biological sources and sinks (green line) represents the balance of O_2 production by photosynthesis and consumption by respiration.

Compared to mean advection and vertical mixing, the eddy advection term contributes modestly to supply O_2 below the mixed layer from 0° - 5°N (Figure 2f and Figure 3b), acting to counteract the negative contribution by the mean upwelling in this region and depth range (50 – 150 m). The positive eddy-driven flux of O_2 into the upper northern equatorial thermocline reflects the integrated effects of transient eddy stirring and downwelling of oxygenated waters by TIVs in this region (Eddebbbar et al., 2021). The role of eddy advection, however, is smaller south of the equator (Figure 2f and Figure 3a) where EKE activity is much weaker (Figure 1d) and less structured (Ubelmann & Fu, 2011). Deeper in the equatorial Pacific thermocline (150-300 m), eddy advection contributes negatively along the equator (2°S - 2°N) to the O_2 budget as the meandering of the EUC and instabilities generated along its path recirculate and stir low- O_2 waters from the neighboring ODZs into the equatorial oxygenated tongue, counteracting the positive contribution by the mean zonal advective supply (Figure 2f and Figure 3). Away from the equator (poleward of 7°N and 7°S), Figure 2f shows that eddies contribute broadly to supply O_2 throughout the oxycline (100-200 m), as similarly found in an O_2 budget study of the Atlantic basin (Calil, 2023).

The critical role of vertical mixing in sustaining O_2 supply in the upper equatorial Pacific thermocline is further illustrated in Figure 3, which shows the vertical profile of the contribution of the budget terms averaged over the southern (7°S - 0°) and northern (0° - 7°N) central and eastern equatorial Pacific. We set our meridional averaging boundaries at 7°S and 7°N to capture the full contribution of eddies and off-equatorial zonal circulation by TIVs and the Tsuchiya jets, respectively. Vertical mixing dominates the O_2 supply from about 50 m to about 120 m below, and remains an important component of the net transport of O_2 down to 150 m depth below which lateral advection becomes the main supply pathway into the eastern and central equatorial Pacific (Figure 3). The pattern of vertical mixing driving O_2 supply in the upper water column and lateral advection dominating at depth is relatively consistent between the eastern and central parts of the equatorial Pacific basin (Figure 2 and Figure S2 in Supporting Information). Some differences between the two regions, however, arise with mixing playing a meridionally more expansive role in the eastern Pacific where the oxycline is shallower (Figure S2d and S2h) while eddy and mean zonal advection play more pronounced roles in the central Pacific (Figure S2b-c and S2f-g) where EKE and the EUC are intensified, respectively.

The outsized role of mixing in the upper equatorial Pacific O_2 budget balance can be attributed to the superposition of i) the pronounced vertical gradient in O_2 set by equatorial upwelling, and ii) the high diffusivity set by the dynamically unique nature of the flow regime along the equatorial Pacific. Within a couple degrees of the equator above the EUC, the high vertical shear between the opposing EUC and SEC (Figure 1d) sustains a marginally stable flow state in the upper ocean characterized by intermittent but strong eddy-mediated turbulent mixing below the base of mixed layer that drives intense heat uptake into the ocean's interior (Moum et al., 2009; Holmes et al., 2019; Cherian et al., 2021; Deppenmeier et al., 2022; Whitt et al., 2022). The spatial extent of the vertical mixing of O_2 shown in Figure 2e is generally similar to previously reported spatial patterns of vertical mixing of heat (Holmes et al., 2019; Deppenmeier et al., 2022; Whitt et al., 2022), with enhanced contributions below the mixed layer (50-150 m) along the cold tongue, and weaker contributions away from the equator associated with turbulent mixing and TIVs (Cherian et al., 2021). A similar role for equatorial turbulence is thus shown here for driving intense local transport of O_2 into the upper thermocline that supplements the advective transport of remotely ventilated waters via the mean zonal and meridional circulation at depth.

4 Seasonal Drivers of Oxygen Supply

The lateral advective and vertical mixing processes driving the renewal and budget balance of O_2 in the equatorial Pacific described in Section 3 are strongly seasonal. Figure 4 shows the seasonal mean O_2 flux from the main supply sources of O_2 into the eastern and central equatorial Pacific thermocline, namely the vertical turbulent mixing flux of O_2 across the mixed layer base integrated over the 7°N - 7°S and 160°W - 80°S area, and the lateral advective fluxes including the mean zonal advective flux across 160°W and the mean equatorward meridional advective flux of O_2 across 7°N and 7°S integrated from the base of the mixed layer base through $\sigma_\theta=26.5 \text{ kg m}^{-3}$. In the analysis of the seasonal variability and mechanisms underlying the vertical mixing flux of O_2 , we focus from here onward on the local mixing flux as parameterized in the KPP scheme (Large et al., 1994), and leave out contributions from the non-local KPP transport term which plays a negligible role in the equatorial Pacific and is thus left out of this discussion for clarity and brevity. Although the total transport of O_2 (gray bar in Figure 4a) varies modestly across seasons (e.g. 46% increase from boreal winter to summer), the individual fluxes comprising this transport vary substantially (~ 160 - 180% change between seasons) and out of phase. During the spring months when vertical mixing and meridional advective fluxes are weak, O_2 supply is dominated by zonal advection (blue in Figure

3a), which sustains a seasonal mean flux of $\sim 5 \times 10^6 \text{ mol s}^{-1}$ primarily via the eastward EUC transport of remotely ventilated waters. Following spring, the downward turbulent mixing of O_2 increases nearly threefold to $\sim 4.5 \times 10^6 \text{ mol s}^{-1}$ during summer and becomes a leading source of O_2 supply in fall (yellow in Figure 4a), contributing substantially to balance the increase in microbial consumption and upwelling during these months (Figure S3 in Supporting Information). Despite their overall weaker magnitudes in winter, mixing and advective fluxes contribute nearly equally during this season, thus sustaining a relatively stable net supply of O_2 year-round in this region (Figure 4a).

The large seasonality of O_2 supply from each of these different pathways is driven mainly by their unique dynamical responses to the annual cycle in the overlying winds. Figure 4c shows the total meridional flux of O_2 (brown line), separated into its northern (dark green) and southern (light green) components, and reveals a strong seasonality in these fluxes that is linked to the variability in the equatorial zonal wind stress (dashed blue line), with increased equatorward transport from late summer through winter when the wind stress is strong, and reduced transport from spring through mid-summer when the wind stress is weak. This seasonal relationship likely reflects the northward migration of the southeasterly winds across the equator during fall and summer, and the subsequent impacts of reduced equatorial wind stress on Ekman surface divergence and the equatorward return flow in the thermocline (Johnson & McPhaden, 1999; Lee & Fukumori, 2003), though changes in wind stress away from the equator may also play a role (Graffino et al., 2019).

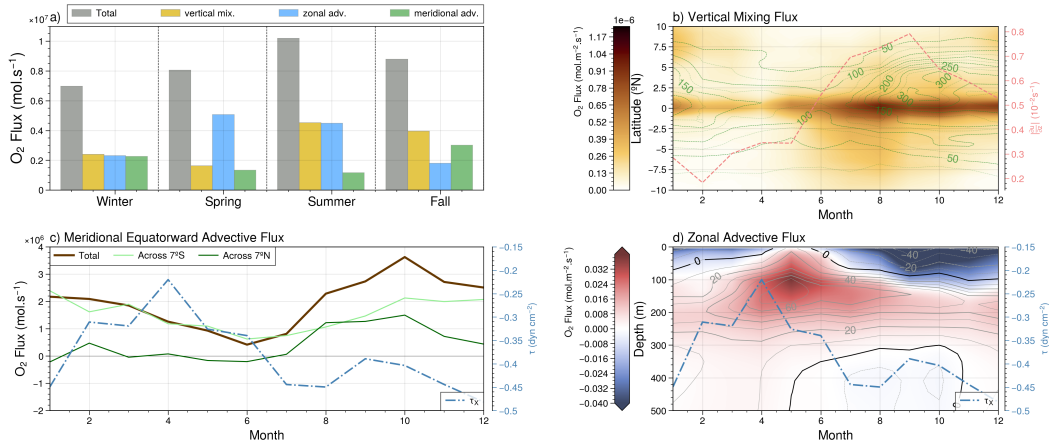


Figure 4. Seasonal drivers of O_2 supply in the upper equatorial Pacific in CESM. a) Seasonal mean fluxes due to vertical mixing (yellow) across the base of the mixed layer integrated over 7°S - 7°N and 80°W - 160°W , zonal advection across 160°W (blue) integrated over 7°S - 7°N from the base of the mixed layer through $\sigma_\theta=26.5 \text{ kg m}^{-3}$, and meridional advection across 7°S and 7°N (green) integrated over 80°W - 160°W from the base of the mixed layer through $\sigma_\theta=26.5 \text{ kg m}^{-3}$, and the sum (grey). b) Hovmöller plot of climatological monthly mean O_2 vertical mixing flux across the mixed layer base averaged zonally over 80°W - 160°W , along with surface EKE ($\text{cm}^2 \text{ s}^{-2}$) in green and $|\frac{\partial u}{\partial z}|$, the absolute vertical shear of zonal velocity averaged over the high shear depth range (80-120 m) from 2°S - 2°N (light red). c) Climatological monthly mean meridional equatorward O_2 flux across 7°S and 7°N , along with equatorial (2°S - 2°N) zonal wind stress (dashed blue) averaged over 80°W - 160°W . Panel d) shows the climatological monthly mean eastward zonal flux of O_2 across 160°W averaged over 7°S to 7°N , along with the equatorial zonal wind stress (dashed blue).

From late winter and through early summer, an intensification and shoaling of the eastward flow by the EUC drives larger zonal fluxes of O_2 into the central and eastern Pacific with corresponding reductions in the magnitude of equatorial wind stress (Figure 4d). This is followed during late summer through early winter by a major slowdown of this zonal supply of O_2 as wind stress intensifies along the equator. This seasonal coupling of the EUC transport to wind forcing (Figure 4d) is likely driven by a complex interaction of zonal wind stress impacts on the zonal pressure gradient, momentum budget, and propagation of Kelvin waves in the equatorial Pacific (Johnson et al., 2002; Kessler, 2006; Sen Gupta et al., 2012).

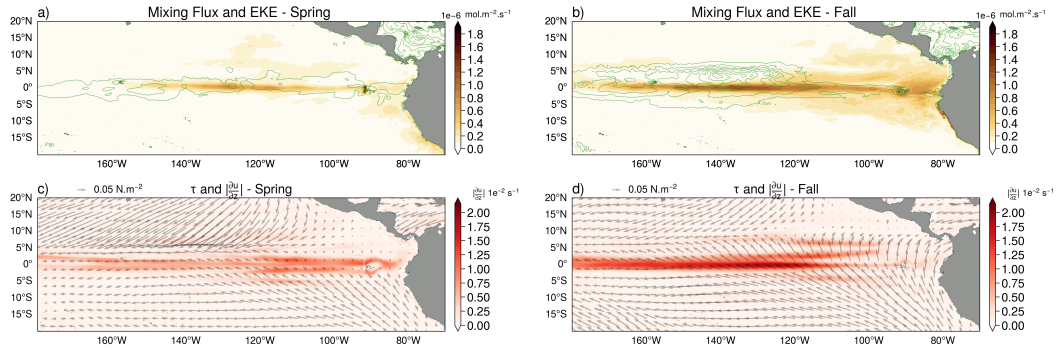


Figure 5. Seasonal mean O_2 flux across the base of the mixed layer due to local vertical mixing along with EKE contoured (green) every $100 \text{ cm}^2 \text{ s}^{-2}$ for a) boreal spring and b) boreal fall in the CESM simulation. Lower panels show the surface wind stress and $|\frac{\partial u}{\partial z}|$, the absolute vertical shear of zonal velocity averaged over the high shear depth range (80-120 m) from 2°S - 2°N , for c) boreal spring and d) boreal fall. The O_2 mixing flux shown in a) and b) represents the maximum value of the local vertical mixing flux below the mixed layer depth (typically 80-120 m). The mixed layer depth is defined in CESM using the buoyancy gradient criteria of Large et al. (1997).

A major consequence of the seasonal cycle in wind forcing is its modulation of the vertical shear in zonal velocity, particularly along the equator where the flow is marginally stable. Figure 4b and Figure 5 detail the latitudinal and seasonal characteristics of the vertical mixing flux of O_2 , which intensifies along the 2°S - 2°N band during summer and fall when the vertical shear of the zonal velocity (dashed red line in Figure 4b and red shading in Figure 5c-d) is highest, and declines substantially during spring when the shear is low. The seasonal and spatial intensity of the vertical mixing flux of O_2 along the equator also co-vary with EKE (green contours in Figure 4b and 5a-b), which increases in summer and fall through the generation and propagation of TIWs and their vortices and reaches its minima in spring when TIWs are typically absent. The seasonal wind forcing of the vertical and lateral shear between the equatorial currents influences both the turbulent mixing in the high shear region (80-120 m) of the EUC as well as the generation of barotropic and baroclinic instabilities in the zonal flow that develop into TIWs, which in turn can influence turbulent mixing (Holmes & Thomas, 2015). This seasonal co-variability of vertical mixing of O_2 with the vertical shear and EKE likely reflects more nuanced and complex interactions across scales, which we explore in the following section.

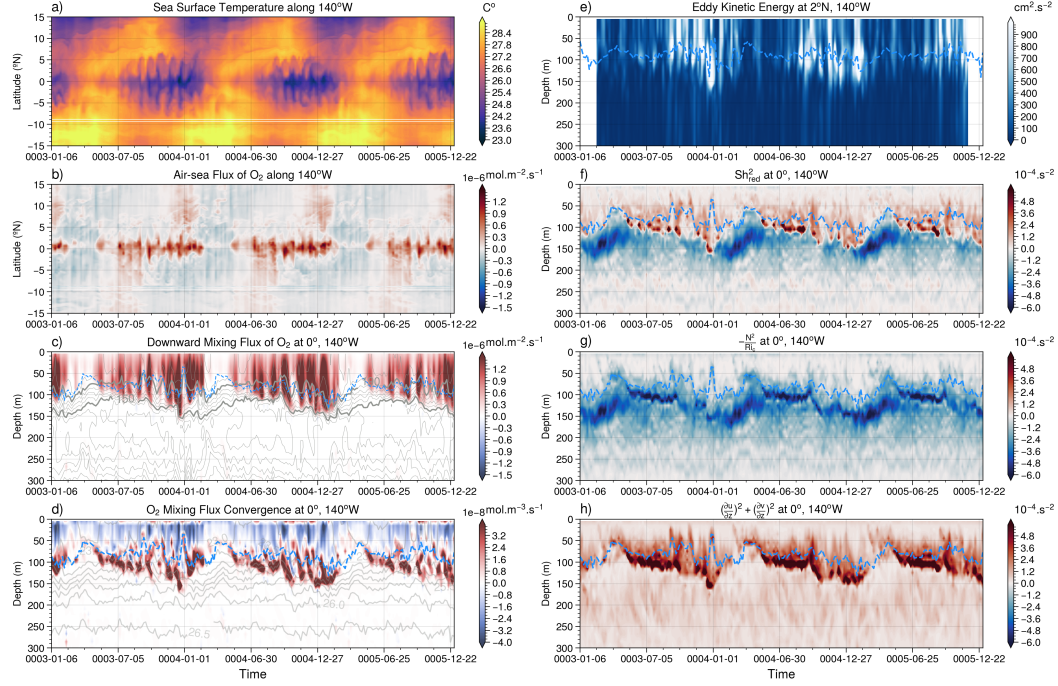


Figure 6. Processes driving TIW modulation of equatorial Pacific O_2 mixing at $140^\circ W$ in CESM. a) Hovmöller plot of a) SST, b) air-sea flux of O_2 , c) downward local mixing flux of O_2 (shading) and O_2 values (grey contours), and d) O_2 local mixing flux convergence (shading) and density layers (grey contours). e) EKE at $2^\circ N$, $140^\circ W$, f) Reduced shear squared, g) Buoyancy frequency scaled by the critical Richardson number, and h) squared vertical shear of the lateral velocity field. Dashed blue line in c) through h) outline the mixed layer depth.

5 Mechanism of Eddy-Mediated Turbulent Mixing of Oxygen

Given its substantial influence on the mean state budget balance and seasonal variability of O_2 supply in the upper equatorial Pacific thermocline, we further examine the underlying drivers of the temporal and spatial structure and variability of vertical mixing of O_2 and its interaction with mesoscale activity in CESM. Figure 6 elucidates the link between the vertical mixing of O_2 and mesoscale activity during the last three years of the CESM simulation at $140^\circ W$ along the equator, a site where shear-driven turbulence and its modulation by eddy dynamics have long been observed and simulated (Chereskin et al., 1986; Halpern et al., 1988; Lien et al., 2008; Moum et al., 2009, 2013; Inoue et al., 2012, 2019; Holmes & Thomas, 2015; Cherian et al., 2021; Whitt et al., 2022). The seasonal intensification of the O_2 mixing flux does not covary with the seasonal shoaling and deepening of the oxycline (Figure 6c), but instead occurs intermittently from summer through mid-winter and coincides with TIW events, outlined by their cold wave-like imprints on SSTs and deep reaching patches of high EKE (Figure 6a, 6c and 6e), while spring showcases little eddy activity or mixing of O_2 . The arrival of TIWs at $140^\circ W$ during summer and fall induces intense surface air-sea fluxes of O_2 near the equator and enhanced downward mixing fluxes of O_2 that penetrate well below the mixed layer down to 150 m depth (Figure 6a-c). The uptake of O_2 due to enhanced mixing is likely buffered though only slightly by thermodynamic effects as TIWs induce an intense air-to-sea flux of heat (Cherian et al., 2021) and a subsequent outgassing of O_2 , similar to ENSO-driven variability in air-sea O_2 flux (Eddebbar et al., 2017). Figure 6d shows that the convergence of this vertical mixing acts to increase O_2 below the mixed layer and throughout the up-

per thermocline ($23.5 < \sigma_\theta < 25.5 \text{ kg.m}^{-3}$). As shown by the logarithmic distribution of the shear-driven turbulent flux of O_2 (Figure S4 in Supporting Information), these intermittent high-shear TIW-mediated mixing events have a considerable influence on setting the mean state of the O_2 vertical mixing and total transport in the upper equatorial Pacific.

The tight link between eddy activity and downward turbulent mixing of O_2 in the equatorial Pacific can be understood in the context of TIW modulation of equatorial turbulence as parameterized in CESM. The upper equatorial Pacific is typically in a state of marginal stability due to the high vertical shear induced by the EUC and SEC, with shear turbulence arising when the vertical shear of lateral velocities prevail over the stabilizing effects of stratification (Smyth & Moum, 2013; Moum, 2021). This subgrid scale turbulence is parameterized as a local shear-driven diffusivity (K_S) in the KPP scheme through a function of the gradient Richardson Number (Ri_g) as follows (Large et al., 1994; Smith et al., 2010):

$$K_S = \begin{cases} K_0, & \text{if } Ri_g < 0 \\ K_0 \left[1 - \left(\frac{Ri_g}{Ri_c} \right)^2 \right]^3, & \text{if } 0 < Ri_g < Ri_c \\ 0, & \text{if } Ri_g > Ri_c \end{cases} \quad (4)$$

where $K_0 = 50 \times 10^{-4} \text{ m}^2 \cdot \text{s}^{-1}$, and Ri_g is calculated as:

$$Ri_g = \frac{N^2}{\left(\frac{\partial u}{\partial z} \right)^2 + \left(\frac{\partial v}{\partial z} \right)^2} \quad (5)$$

where $N^2 = \frac{\partial b}{\partial z}$ is the buoyancy frequency squared, $b = -\frac{g\rho}{\rho_0}$ is the buoyancy, and $\left(\frac{\partial u}{\partial z} \right)^2 + \left(\frac{\partial v}{\partial z} \right)^2$ is the sum of the squared shears in zonal and meridional velocities. Ri_c refers to a critical Ri threshold, set here at 0.8, a value that most consistently yields the diffusive mixing from resolved turbulence in the equatorial regime in Large Eddy Simulation (LES) experiments (Large & Gent, 1999). When the Ri_g falls below Ri_c , shear instabilities develop and K_S steeply increases towards the maximum value of K_0 . When Ri_g values exceed Ri_c , shear instabilities are inactive and K_S is set to 0. A key metric for quantifying the contribution of changes in stratification vs vertical shear in inducing turbulence is the reduced shear squared (Sh_{red}), calculated as:

$$Sh_{red}^2 = \left(\frac{\partial u}{\partial z} \right)^2 + \left(\frac{\partial v}{\partial z} \right)^2 - \frac{N^2}{Ri_c} \quad (6)$$

where N^2 is normalized by Ri_c following Cherian et al. (2021) and acts to stabilize the flow, while $\left(\frac{\partial u}{\partial z} \right)^2 + \left(\frac{\partial v}{\partial z} \right)^2$ acts to destabilize it. Positive values of Sh_{red} indicate periods when the flow is turbulent ($Ri_g < Ri_c$), and are outlined in Figure 6f as intense positive (red) patches (Figure 6f) where variations in the vertical shear in lateral velocities overcome the stratification effects (Figure 6g-h). These marked increases in the vertical shear are tightly coupled to the intensification of EKE via the westward passage of TIWs (Figure 6e-h) and their vortex stretching effects (Holmes & Thomas, 2015; Inoue et al., 2019), which push the flow state towards instability. As TIWs propagate westward through 140°W , K_S increases rapidly and combined with the pronounced vertical gradient of O_2 in the upper thermocline, the downward mixing flux of O_2 is significantly intensified (Figure 6). The reduction of EKE when TIWs are largely inactive (e.g. during spring) and the subsequent weakening of the vertical shear bring the flow back towards a stable state ($Ri_g > Ri_c$), substantially weakening the vertical diffusive flux of O_2 during such periods (Figure 6).

We further illustrate the spatial structure of how TIWs impacts the downward turbulent mixing of O_2 in Figure 7, which shows a 5-day mean snapshot of the air-sea flux,

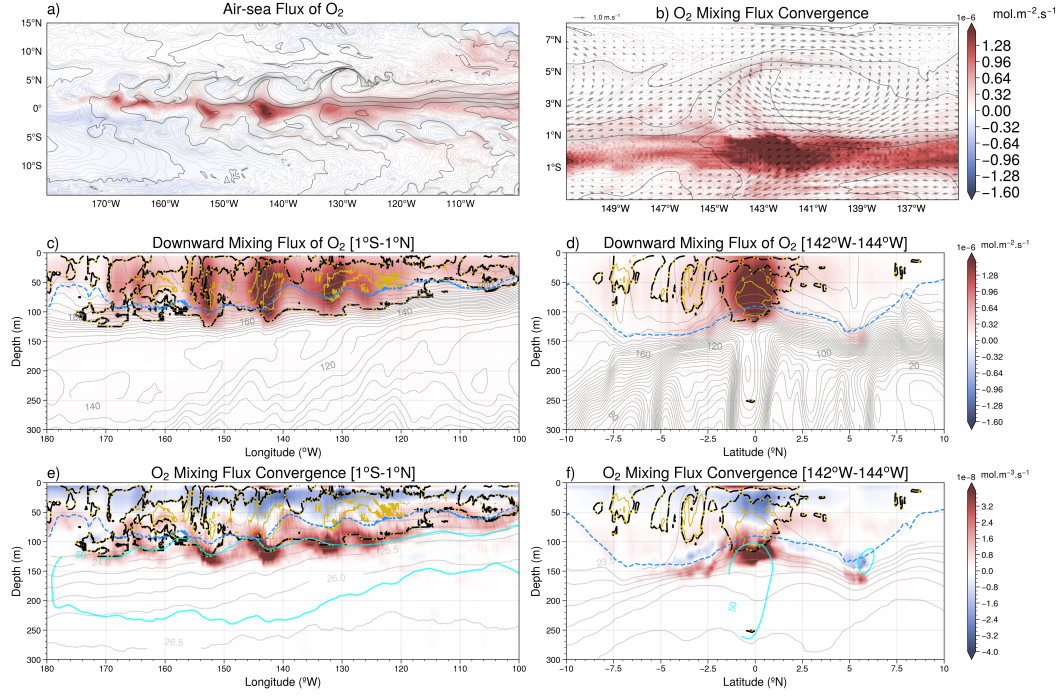


Figure 7. Eddy-Mediated Mixing of Oxygen. 5-day mean values around October 3, of year 5 of the CESM simulation of a) air-sea flux of O_2 and SST (contoured every 1° in bold and 0.1 in light), b) local mixing flux convergence integrated from the base of the mixed layer through the 26.5 isopycnal and horizontal velocity at 50 m depth zoomed on a TIW centered around $143^\circ W$. Panels c) and d) show the downward local mixing flux of O_2 averaged over $1^\circ S$ - $1^\circ N$ and $142^\circ W$ - $144^\circ W$ (color shading), respectively, along with the low Ri layer contoured at the critical value in POP2 at 0.8 (dashed black and yellow) and 0.4 (yellow), mixed layer in dashed blue, and O_2 contours in light gray. Panels e) and f) show the O_2 local mixing flux convergence averaged over $1^\circ S$ - $1^\circ N$ and $142^\circ W$ - $144^\circ W$ (color shading), respectively, along with the low Ri layer (dashed black and yellow), isopycnals (gray contours), mixed layer (dashed blue), and the 50 cm s^{-1} zonal velocity contour outlining the EUC region of high shear (cyan).

local vertical mixing flux, and the convergence of the vertical mixing flux of O_2 during a period when TIWs were active. Intense patches of air-sea flux and downward mixing flux are co-located with the cold cores of TIWs along the equator (Figure 7a-d). Below the surface, turbulent regions outlined by Ri_c contours (black and yellow) coincide with these cores throughout the upper 120m between $2^\circ S$ and $2^\circ N$, and showcase an intense mixing flux of O_2 and maxima in the vertical convergence of this flux that reach well below the mixed layer and into the core of the EUC (Figure 7e-f). Figure 6 and 7 thus suggest that mesoscale eddies sustain a fast and intense vertical pathway of O_2 exchange from the surface to the thermocline via the TIW modulation of shear instability. The integrated effects of this intermittent TIW-mediated mixing of O_2 leads to a substantial injection of O_2 over the eddy lifetimes with considerable influence on the steady state and seasonal O_2 budget balance (Figures 2-4).

6 Summary and Discussion

Our eddy-resolving model analysis of the equatorial Pacific O_2 budget reveals that turbulent mixing and its modulation by mesoscale eddies play a critical role in supplying O_2 to the upper (50-150 m) thermocline. This O_2 supply acts to augment the previously reported replenishment of O_2 by the EUC, Tsuchiya jets, and meridional circulation deeper (150-300 m) in the thermocline (Stramma et al., 2010; Busecke et al., 2019; Margolskee et al., 2019; Duteil et al., 2014), and suggests that both advective and mixing processes and their interplay sustain the ventilation of the equatorial Pacific thermocline and the presence of the equatorial oxygenated tongue separating the tropical Pacific ODZs. Our Reynolds decomposition further shows that mesoscale eddies play a spatially complex but relatively minor direct role through their eddy advection effects in the equatorial Pacific O_2 budget balance, supplying O_2 along the high EKE region of the upper equatorial Pacific (down to 150 m) and reducing O_2 along the EUC path at depth (150-300 m). These mixing and advective sources of O_2 are highly seasonal and are driven by the annual cycle in surface wind forcing which i) modulates the magnitude of lateral advection of remotely ventilated waters into the central and eastern equatorial Pacific, and ii) controls the seasonality in EKE and vertical shear of the zonal flow that drives the local downward mixing of O_2 . We further examine the processes underlying the vertical mixing of O_2 and its relationship to eddy activity, and find that TIWs strongly modulate the turbulent flux of O_2 via their eddy impact on the vertical shear in lateral velocities. Thus, while eddies play a relatively minor role in the equatorial Pacific O_2 budget balance through their direct eddy advection effects, they play a large indirect role in supplying O_2 into the upper thermocline via their modulation of equatorial shear instability, which sustains a local ventilation pathway of O_2 from the surface layer to the ocean's interior.

These interactions across processes and scales - from basin-wide currents and mesoscale eddies to fine scale turbulence - underscore the complexity by which past and future changes in the equatorial Pacific O_2 content must be approached. These changes should reflect not only the temperature dependence of gas solubility and changes in remote ventilation via the equatorial current system, but also how local ventilation via turbulent mixing and its modulation by eddies will shift as the tropical Pacific ocean responds to anthropogenic radiative forcing (Vecchi et al., 2006; Ying et al., 2022). Our results also have implications for identifying the source of the underestimate in the interannual variability and long-term trends of O_2 in climate models (Oschlies et al., 2018), where eddies and their impacts on turbulence are not resolved. Finally, the shear-driven downward turbulent flux of heat and O_2 along the equatorial Pacific cold tongue suggests the existence of a positive relationship between air-sea O_2 and heat fluxes. This positive coupling stands in contrast to their well-established negative relationship over most of the world ocean from seasonal to multi-decadal timescales (Garcia & Keeling, 2001; Bopp et al., 2002; Keeling & Garcia, 2002; Keeling et al., 2010; Ito et al., 2017), and suggests that heat uptake can co-occur with increased O_2 in the equatorial Pacific thermocline.

An important caveat underlying our model-based analysis is that turbulent mixing is parameterized in our model, and that the magnitude of this term and its impacts on tracer transport away from the equator and $140^\circ W$ is not well known. A study by Zaron and Moum (2009) further suggests that KPP may overestimate the magnitude of mixing by shear instability in the equatorial region, potentially overestimating the downward turbulent flux of heat in CESM (Deppenmeier et al., 2022), and other important tracers (e.g. O_2). Additionally, our model doesn't resolve or parameterize other sources of mixing stemming from mesoscale circulation, e.g. the cascade of TIW-induced internal lee waves to turbulence (Tanaka et al., 2015), which may have relevant consequences for mixing further down the thermocline near the ODZ boundaries. Future simulations using different mixing schemes along with comparison across models of finer resolution, including higher resolution regional simulations of the equatorial Pacific and Large Eddy

Simulations with biogeochemistry, will be key to quantify the sensitivity of our results to model choice, parameterization scheme, and model resolution. Most importantly, sustained fine scale observations of mixing and biogeochemical tracers such as O_2 along the equator are needed to quantify the intensity and spatial structure of mixing and its impacts on O_2 variability from diurnal to multi-annual timescales in this region.

Nevertheless, the interplay of eddy activity and parameterized shear-driven mixing permitted by the high resolution grid employed in this configuration of CESM presents new insights into interactions of ocean dynamics and biogeochemistry. The role of eddy-mediated mixing in driving downward transport of heat and O_2 may have analogous but inverse impacts on the upward transport of nutrients and carbon from the EUC to the surface layer, with potentially important implications for modulating the outgassing of carbon and productivity in this region. Dedicated physical-biogeochemical field campaigns and enhanced biogeochemical observations targeting TIWs phenomena are particularly needed to test these model-based findings in nature.

7 Open Research

The CESM model code is publicly available at <https://www.cesm.ucar.edu/models>. Processed model outputs and analysis code used to complete this work are available on Zenodo at doi.org/10.5281/zenodo.8371745 and doi.org/10.5281/zenodo.8339521.

Acknowledgments

The authors acknowledge support from the National Science Foundation OCE grant number 1948599 and high-performance computing support from Cheyenne provided by NCAR's Computational and Information Systems Laboratory, sponsored by NSF. DBW acknowledges support from the NASA Physical Oceanography and Salinity Science programs and NASA award NIP20-0113.

References

- Bettencourt, J. H., López, C., Hernández-García, E., Montes, I., Sudre, J., Dewitte, B., ... Garçon, V. (2015). Boundaries of the peruvian oxygen minimum zone shaped by coherent mesoscale dynamics. *Nature Geoscience*, 8(12), 937.
- Bopp, L., Le Quéré, C., Heimann, M., Manning, A. C., & Monfray, P. (2002). Climate-induced oceanic oxygen fluxes: Implications for the contemporary carbon budget. *Global Biogeochemical Cycles*, 16(2), 6–1.
- Brandt, P., Bange, H. W., Banyte, D., Dengler, M., Didwischus, S.-H., Fischer, T., ... Visbeck, M. (2015). On the role of circulation and mixing in the ventilation of oxygen minimum zones with a focus on the eastern tropical north atlantic. *Biogeosciences (BG)*, 12, 489–512.
- Brandt, P., Hahn, J., Schmidtke, S., Tuchen, F. P., Kopte, R., Kiko, R., ... Dengler, M. (2021). Atlantic equatorial undercurrent intensification counteracts warming-induced deoxygenation. *Nature Geoscience*, 14(5), 278–282.
- Busecke, J. J., Resplandy, L., Ditzovsky, S. J., & John, J. G. (2022). Diverging fates of the pacific ocean oxygen minimum zone and its core in a warming world. *AGU Advances*, 3(6), e2021AV000470.
- Busecke, J. J., Resplandy, L., & Dunne, J. P. (2019). The equatorial undercurrent and the oxygen minimum zone in the pacific. *Geophysical Research Letters*, 46(12), 6716–6725.
- Cabré, A., Marinov, I., Bernardello, R., & Bianchi, D. (2015). Oxygen minimum zones in the tropical pacific across cmip5 models: mean state differences and climate change trends. *Biogeosciences*, 12(18), 5429–5454.
- Calil, P. H. (2023). High-resolution, basin-scale simulations reveal the impact of intermediate zonal jets on the atlantic oxygen minimum zones. *Journal of Advances in Modeling Earth Systems*, 15(2), e2022MS003158.
- Chereskin, T., Moum, J. N., Staben, P., Caldwell, D. R., Paulson, C., Regier, L., & Halpern, D. (1986). Fine-scale variability at 140° w in the equatorial pacific. *Journal of Geophysical Research: Oceans*, 91(C11), 12887–12897.
- Cherian, D., Whitt, D., Holmes, R., Lien, R.-C., Bachman, S., & Large, W. (2021). Off-equatorial deep-cycle turbulence forced by tropical instability waves in the equatorial pacific. *Journal of Physical Oceanography*, 51(5), 1575–1593.
- Couespel, D., Lévy, M., & Bopp, L. (2019). Major contribution of reduced upper ocean oxygen mixing to global ocean deoxygenation in an earth system model. *Geophysical Research Letters*, 46(21), 12239–12249.
- Deppenmeier, A.-L., Bryan, F. O., Kessler, W. S., & Thompson, L. (2022). Diabatic upwelling in the tropical pacific: Seasonal and subseasonal variability. *Journal of Physical Oceanography*, 52(11), 2657–2668.
- Drenkard, E. J., & Karnauskas, K. B. (2014). Strengthening of the pacific equatorial undercurrent in the soda reanalysis: Mechanisms, ocean dynamics, and implications. *Journal of Climate*, 27(6), 2405–2416.
- Duteil, O., Böning, C. W., & Oschlies, A. (2014). Variability in subtropical-tropical cells drives oxygen levels in the tropical pacific ocean. *Geophysical Research Letters*, 41(24), 8926–8934.
- Eddebbar, Y., Long, M. C., Resplandy, L., Rödenbeck, C., Rodgers, K. B., Manizza, M., & Keeling, R. F. (2017). Impacts of enso on air-sea oxygen exchange: Observations and mechanisms. *Global Biogeochemical Cycles*, 31(5), 901–921.
- Eddebbar, Y., Subramanian, A., Whitt, D., Long, M., Verdy, A., Mazloff, M., & Merrifield, M. (2021). Seasonal modulation of dissolved oxygen in the equatorial pacific by tropical instability vortices. *Journal of Geophysical Research: Oceans*, 126(11), e2021JC017567.
- Frenger, I., Bianchi, D., Stührenberg, C., Oschlies, A., Dunne, J., Deutsch, C., ... Schütte, F. (2018). Biogeochemical role of subsurface coherent eddies in the ocean: Tracer cannonballs, hypoxic storms, and microbial stewpots? *Global Biogeochemical Cycles*, 32(2), 226–249.

- Gallo, N., & Levin, L. (2016). Fish ecology and evolution in the world's oxygen minimum zones and implications of ocean deoxygenation. In *Advances in marine biology* (Vol. 74, pp. 117–198). Elsevier.
- Garcia, H. E., Boyer, T. P., Levitus, S., Locarnini, R. A., & Antonov, J. (2005). On the variability of dissolved oxygen and apparent oxygen utilization content for the upper world ocean: 1955 to 1998. *Geophysical Research Letters*, 32(9).
- Garcia, H. E., & Keeling, R. F. (2001). On the global oxygen anomaly and air-sea flux. *Journal of Geophysical Research: Oceans*, 106(C12), 31155–31166.
- Gouretski, V., & Koltermann, K. P. (2004). Woce global hydrographic climatology. *Berichte des BSH*, 35, 1–52.
- Graffino, G., Farneti, R., Kucharski, F., & Molteni, F. (2019). The effect of wind stress anomalies and location in driving pacific subtropical cells and tropical climate. *Journal of Climate*, 32(5), 1641–1660.
- Gray, J. S., Wu, R. S.-s., & Or, Y. Y. (2002). Effects of hypoxia and organic enrichment on the coastal marine environment. *Marine ecology progress series*, 238, 249–279.
- Griffies, S. M., Biastoch, A., Bärning, C., Bryan, F., Danabasoglu, G., Chassignet, E. P., . . . Yin, J. (2009). Coordinated ocean-ice reference experiments (cores). *Ocean modelling*, 26(1-2), 1–46.
- Hahn, J., Brandt, P., Greatbatch, R. J., Krahmann, G., & Körtzinger, A. (2014). Oxygen variance and meridional oxygen supply in the tropical north east atlantic oxygen minimum zone. *Climate Dynamics*, 43, 2999–3024.
- Halpern, D., Knox, R. A., & Luther, D. S. (1988). Observations of 20-day period meridional current oscillations in the upper ocean along the pacific equator. *Journal of Physical Oceanography*, 18(11), 1514–1534.
- Harrison, C. S., Long, M. C., Lovenduski, N. S., & Moore, J. K. (2018). Mesoscale effects on carbon export: a global perspective. *Global Biogeochemical Cycles*, 32(4), 680–703.
- Holmes, R., McGregor, S., Santoso, A., & England, M. H. (2019). Contribution of tropical instability waves to enso irregularity. *Climate Dynamics*, 52(3-4), 1837–1855.
- Holmes, R., & Thomas, L. (2015). The modulation of equatorial turbulence by tropical instability waves in a regional ocean model. *Journal of Physical Oceanography*, 45(4), 1155–1173.
- Inoue, R., Lien, R.-C., & Moum, J. (2012). Modulation of equatorial turbulence by a tropical instability wave. *Journal of Geophysical Research: Oceans*, 117(C10).
- Inoue, R., Lien, R.-C., Moum, J. N., Perez, R. C., & Gregg, M. C. (2019). Variations of equatorial shear, stratification, and turbulence within a tropical instability wave cycle. *Journal of Geophysical Research: Oceans*, 124(3), 1858–1875.
- Ito, T., Minobe, S., Long, M. C., & Deutsch, C. (2017). Upper ocean o₂ trends: 1958–2015. *Geophysical Research Letters*, 44(9), 4214–4223.
- Johnson, G. C., & McPhaden, M. J. (1999). Interior pycnocline flow from the subtropical to the equatorial pacific ocean. *Journal of Physical Oceanography*, 29(12), 3073–3089.
- Johnson, G. C., Sloyan, B. M., Kessler, W. S., & McTaggart, K. E. (2002). Direct measurements of upper ocean currents and water properties across the tropical pacific during the 1990s. *Progress in Oceanography*, 52(1), 31–61.
- Karstensen, J., Stramma, L., & Visbeck, M. (2008). Oxygen minimum zones in the eastern tropical atlantic and pacific oceans. *Progress in Oceanography*, 77(4), 331–350.
- Keeling, R. F., & Garcia, H. E. (2002). The change in oceanic o₂ inventory associated with recent global warming. *Proceedings of the National Academy of Sciences*, 99(12), 7848–7853.

- Keeling, R. F., Körtzinger, A., & Gruber, N. (2010). Ocean deoxygenation in a warming world. *Annual review of marine science*, 2, 199–229.
- Kennan, S. C., & Flament, P. J. (2000). Observations of a tropical instability vortex. *Journal of Physical Oceanography*, 30(9), 2277–2301.
- Kessler, W. S. (2006). The circulation of the eastern tropical pacific: A review. *Progress in Oceanography*, 69(2-4), 181–217.
- Large, W. G., Danabasoglu, G., Doney, S. C., & McWilliams, J. C. (1997). Sensitivity to surface forcing and boundary layer mixing in a global ocean model: Annual-mean climatology. *Journal of Physical Oceanography*, 27(11), 2418–2447.
- Large, W. G., & Gent, P. R. (1999). Validation of vertical mixing in an equatorial ocean model using large eddy simulations and observations. *Journal of Physical Oceanography*, 29(3), 449–464.
- Large, W. G., McWilliams, J. C., & Doney, S. C. (1994). Oceanic vertical mixing: A review and a model with a nonlocal boundary layer parameterization. *Reviews of Geophysics*, 32(4), 363–403.
- Large, W. G., & Yeager, S. G. (2004). *Diurnal to decadal global forcing for ocean and sea-ice models: The data sets and flux climatologies*. National Center for Atmospheric Research Boulder.
- Lee, T., & Fukumori, I. (2003). Interannual-to-decadal variations of tropical–subtropical exchange in the pacific ocean: Boundary versus interior pycnocline transports. *Journal of Climate*, 16(24), 4022–4042.
- Lévy, M., Resplandy, L., Palter, J. B., Couespel, D., & Lachkar, Z. (2022). The crucial contribution of mixing to present and future ocean oxygen distribution. In *Ocean mixing* (pp. 329–344). Elsevier.
- Lien, R.-C., d’Asaro, E. A., & Menkes, C. E. (2008). Modulation of equatorial turbulence by tropical instability waves. *Geophysical Research Letters*, 35(24).
- Long, M. C., Lindsay, K., Peacock, S., Moore, J. K., & Doney, S. C. (2013). Twentieth-century oceanic carbon uptake and storage in cesm1 (bgc). *Journal of Climate*, 26(18), 6775–6800.
- Margolskee, A., Frenzel, H., Emerson, S., & Deutsch, C. (2019). Ventilation pathways for the north pacific oxygen deficient zone. *Global Biogeochemical Cycles*, 33(7), 875–890.
- McGillicuddy Jr, D., Anderson, L., Doney, S., & Maltrud, M. (2003). Eddy-driven sources and sinks of nutrients in the upper ocean: Results from a 0.1 resolution model of the north atlantic. *Global Biogeochemical Cycles*, 17(2).
- Moore, J. K., Lindsay, K., Doney, S. C., Long, M. C., & Misumi, K. (2013). Marine ecosystem dynamics and biogeochemical cycling in the community earth system model [cesm1 (bgc)]: Comparison of the 1990s with the 2090s under the rcp4. 5 and rcp8. 5 scenarios. *Journal of Climate*, 26(23), 9291–9312.
- Moum, J. (2021). Variations in ocean mixing from seconds to years. *Annual Review of Marine Science*, 13, 201–226.
- Moum, J., Lien, R.-C., Perlin, A., Nash, J., Gregg, M., & Wiles, P. (2009). Sea surface cooling at the equator by subsurface mixing in tropical instability waves. *Nature Geoscience*, 2(11), 761–765.
- Moum, J., Perlin, A., Nash, J. D., & McPhaden, M. J. (2013). Seasonal sea surface cooling in the equatorial pacific cold tongue controlled by ocean mixing. *Nature*, 500(7460), 64–67.
- Oschlies, A., Brandt, P., Stramma, L., & Schmidtko, S. (2018). Drivers and mechanisms of ocean deoxygenation. *Nature Geoscience*, 11(7), 467–473.
- Portela, E., Kolodziejczyk, N., Vic, C., & Thierry, V. (2020). Physical mechanisms driving oxygen subduction in the global ocean. *Geophysical Research Letters*, 47(17), e2020GL089040.
- Rohr, T., Harrison, C., Long, M. C., Gaube, P., & Doney, S. C. (2020). The simulated biological response to southern ocean eddies via biological rate

- modification and physical transport. *Global Biogeochemical Cycles*, 34(6), e2019GB006385.
- Ryan, J. P., Ueki, I., Chao, Y., Zhang, H., Polito, P. S., & Chavez, F. P. (2006). Western pacific modulation of large phytoplankton blooms in the central and eastern equatorial pacific. *Journal of Geophysical Research: Biogeosciences*, 111(G2).
- Schmidtko, S., Stramma, L., & Visbeck, M. (2017). Decline in global oceanic oxygen content during the past five decades. *Nature*, 542(7641), 335.
- Sen Gupta, A., Ganachaud, A., McGregor, S., Brown, J. N., & Muir, L. (2012). Drivers of the projected changes to the pacific ocean equatorial circulation. *Geophysical Research Letters*, 39(9).
- Smith, R., Jones, P., Briegleb, B., Bryan, F., Danabasoglu, G., Dennis, J., ... Hecht, M. (2010). The parallel ocean program (pop) reference manual: ocean component of the community climate system model (ccsm) and community earth system model (cesm). *Rep. LAUR-01853*, 141, 1–140.
- Smyth, W., & Moum, J. (2013). Marginal instability and deep cycle turbulence in the eastern equatorial pacific ocean. *Geophysical Research Letters*, 40(23), 6181–6185.
- Song, H., Long, M. C., Gaube, P., Frenger, I., Marshall, J., & McGillicuddy Jr, D. J. (2018). Seasonal variation in the correlation between anomalies of sea level and chlorophyll in the antarctic circumpolar current. *Geophysical Research Letters*, 45(10), 5011–5019.
- Stramma, L., Johnson, G. C., Firing, E., & Schmidtko, S. (2010). Eastern pacific oxygen minimum zones: Supply paths and multidecadal changes. *Journal of Geophysical Research: Oceans*, 115(C9).
- Stramma, L., Prince, E. D., Schmidtko, S., Luo, J., Hoolihan, J. P., Visbeck, M., ... Körtzinger, A. (2012). Expansion of oxygen minimum zones may reduce available habitat for tropical pelagic fishes. *Nature Climate Change*, 2(1), 33.
- Strutton, P. G., Palacz, A. P., Dugdale, R. C., Chai, F., Marchi, A., Parker, A. E., ... Wilkerson, F. P. (2011). The impact of equatorial pacific tropical instability waves on hydrography and nutrients: 2004–2005. *Deep Sea Research Part II: Topical Studies in Oceanography*, 58(3–4), 284–295.
- Strutton, P. G., Ryan, J. P., & Chavez, F. P. (2001). Enhanced chlorophyll associated with tropical instability waves in the equatorial pacific. *Geophysical Research Letters*, 28(10), 2005–2008.
- Sverdrup, H. (1938). On the explanation of the oxygen minima and maxima in the oceans. *ICES Journal of Marine Science*, 13(2), 163–172.
- Tanaka, Y., Hibiya, T., & Sasaki, H. (2015). Downward lee wave radiation from tropical instability waves in the central equatorial pacific ocean: A possible energy pathway to turbulent mixing. *Journal of Geophysical Research: Oceans*, 120(11), 7137–7149.
- Tian, F., Zhang, R.-H., & Wang, X. (2018). A coupled ocean physics-biology modeling study on tropical instability wave-induced chlorophyll impacts in the pacific. *Journal of Geophysical Research: Oceans*, 123(8), 5160–5179.
- Ubelmann, C., & Fu, L.-L. (2011). Vorticity structures in the tropical pacific from a numerical simulation. *Journal of physical oceanography*, 41(8), 1455–1464.
- Vaquer-Sunyer, R., & Duarte, C. M. (2008). Thresholds of hypoxia for marine biodiversity. *Proceedings of the National Academy of Sciences*, 105(40), 15452–15457.
- Vecchi, G. A., Soden, B. J., Wittenberg, A. T., Held, I. M., Leetmaa, A., & Harrison, M. J. (2006). Weakening of tropical pacific atmospheric circulation due to anthropogenic forcing. *Nature*, 441(7089), 73–76.
- Vichi, M., Masina, S., & Nencioli, F. (2008). A process-oriented model study of equatorial pacific phytoplankton: the role of iron supply and tropical instability waves. *Progress in Oceanography*, 78(2), 147–162.

- 729 Whitt, D., Cherian, D., Holmes, R., Bachman, S., Lien, R.-C., Large, W., & Moum,
730 J. (2022). Simulation and scaling of the turbulent vertical heat transport and
731 deep-cycle turbulence across the equatorial pacific cold tongue. *Journal of*
732 *Physical Oceanography*, 52(5), 981–1014.
- 733 Willett, C. S., Leben, R. R., & Lavín, M. F. (2006). Eddies and tropical instabil-
734 ity waves in the eastern tropical pacific: A review. *Progress in Oceanography*,
735 69(2-4), 218–238.
- 736 Wyrski, K. (1962). The oxygen minima in relation to ocean circulation. In *Deep sea*
737 *research and oceanographic abstracts* (Vol. 9, pp. 11–23).
- 738 Ying, J., Collins, M., Cai, W., Timmermann, A., Huang, P., Chen, D., & Stein, K.
739 (2022). Emergence of climate change in the tropical pacific. *Nature Climate*
740 *Change*, 12(4), 356–364.
- 741 Zaron, E. D., & Moum, J. N. (2009). A new look at richardson number mixing
742 schemes for equatorial ocean modeling. *Journal of physical oceanography*,
743 39(10), 2652–2664.

Eddy-Mediated Mixing of Oxygen in the Equatorial Pacific

Yassir A. Eddebbar¹, Daniel B. Whitt², Ariane Verdy¹, Matthew R. Mazloff¹,
Aneesh C. Subramanian³, Matthew C. Long⁴

¹Scripps Institution of Oceanography, University of California San Diego, La Jolla, CA

²Ames Research Center, NASA, Moffett Field, CA

³Atmospheric and Oceanic Sciences, Colorado University, Boulder, CO

⁴National Center for Atmospheric Research, Boulder, CO

Key Points:

- Vertical mixing is an important source of oxygen supply to the upper equatorial Pacific thermocline.
- The simulated supply of oxygen by advection and vertical mixing is strongly seasonal and is driven by seasonal variability in the wind.
- The vertical mixing of oxygen is strongly modulated by the simulated mesoscale eddy impacts on equatorial shear-driven turbulence.

Corresponding author: Yassir Eddebbar, yeddebba@ucsd.edu

Abstract

In the tropical Pacific, weak ventilation and intense microbial respiration at depth give rise to a low dissolved oxygen (O_2) environment that is thought to be ventilated primarily by the equatorial current system (ECS). The role of mesoscale eddies and diapycnal mixing as potential pathways of O_2 supply in this region, however, remains poorly known due to sparse observations and coarse model resolution. Using an eddy resolving simulation of ocean circulation and biogeochemistry, we assess the contribution of these processes to the O_2 budget balance and find that turbulent mixing of O_2 and its modulation by mesoscale eddies contribute substantially to the replenishment of O_2 in the upper equatorial Pacific thermocline, complementing the advective supply of O_2 by the ECS and meridional circulation at depth. These transport processes are strongly sensitive to seasonal forcing by the wind, with elevated mixing of O_2 into the upper thermocline during summer and fall when the vertical shear of the lateral flow and eddy kinetic energy are intensified. The tight link between eddy activity and the downward mixing of O_2 arises from the modulation of equatorial turbulence by Tropical Instability Waves via their eddy impacts on the vertical shear. This interaction of ocean processes across scales sustains a local pathway of O_2 delivery into the equatorial Pacific interior and highlights the need for adequate observations and model representation of turbulent mixing and mesoscale processes for understanding and predicting the fate of the tropical Pacific O_2 content in a warmer and more stratified ocean.

Plain Language Summary

The eastern tropical Pacific interior is an O_2 deficient environment, due to intense O_2 consumption by microbial communities that is not vigorously replenished by ocean circulation at depth. In this study, we use a high resolution simulation of ocean circulation and biogeochemistry to understand the role of finer scale processes such as turbulence and eddies in injecting O_2 locally. We find that mixing due to turbulence along the equator supplies a key portion of O_2 into the ocean by exchanging waters between the well-aerated mixed layer near the surface and the ocean's interior where O_2 falls precipitously with depth. We also find that this mixing varies considerably with the seasons. This annual cycle in mixing arises from the seasonal passage of eddies, which amplifies turbulence through their influence on the subsurface currents along the equator, and represents a previously unexplored but potentially important route of O_2 delivery into the ocean's interior. As the upper ocean warms and becomes less dense, the ocean's O_2 content is expected to decrease, and thus observing and accurately modeling these O_2 pathways will be crucial to monitoring how marine ecosystem habitats will shift in a warmer climate.

1 Introduction

Aerobic marine organisms in the tropical Pacific navigate a complex habitat, set by high productivity in the euphotic layer along the upwelling regions and scarce dissolved oxygen (O_2) at depth. This O_2 scarcity is set by a net balance of weak O_2 supply and intense microbial consumption in the thermocline (Sverdrup, 1938; Wyrski, 1962; Karstensen et al., 2008), giving rise to large O_2 deficient zones (ODZs) at depth where O_2 levels fall below hypoxic thresholds (Gray et al., 2002; Vaquer-Sunyer & Duarte, 2008). These ODZs have exhibited a concerning expansion in recent decades, threatening to further compress the ecosystem habitats and foraging range of pelagic fisheries (Stramma et al., 2012; Gallo & Levin, 2016). Though O_2 decline at high and mid-latitudes is expected due to the sensitivity of O_2 solubility and ocean ventilation to warming (Keeling et al., 2010), a mechanistic explanation for the observed tropical Pacific O_2 loss is lacking due to poor understanding of the processes governing O_2 supply and its variability in this region (Brandt et al., 2015; Oschlies et al., 2018). This is especially evident in the equatorial Pacific which accounts for the largest reported O_2 loss globally in recent decades (Schmidtke et al., 2017) and where the energetic circulation (Figure 1) exerts a complex and poorly understood influence on O_2 structure and variability (Stramma et al., 2010; Margolskee et al., 2019; Busecke et al., 2019).

The reported O_2 decline in the equatorial Pacific of 210 ± 125 Tmol per decade since 1960 (Schmidtke et al., 2017) has coincided with a multidecadal strengthening of the Equatorial Undercurrent (EUC) (Drenkard & Karneuskas, 2014). This is puzzling given the EUC's role as the main pathway of O_2 supply to the central and eastern equatorial Pacific (Stramma et al., 2010; Busecke et al., 2019): an intensification of the EUC would be expected to increase O_2 levels in the eastern and central equatorial Pacific, as analogously shown by the strengthening of the Atlantic EUC and its subsequent oxygenation of the upper equatorial Atlantic (Brandt et al., 2021). The EUC, however, is also a major source of nutrients to the eastern and central equatorial Pacific (Ryan et al., 2006), which can indirectly influence O_2 levels by fueling productivity at the surface and intensifying consumption at depth. O_2 is also supplied via the north and south subsurface counter-currents ("Tsuchiya" jets) and the intermediate counter-currents, and though their volume transport is much weaker than the EUC, these jets represent important ventilation pathways due to their deeper isopycnal range and their off-equator deflection into the ODZ regions (Stramma et al., 2010; Margolskee et al., 2019).

A potentially important but less explored pathway of O_2 supply in the equatorial Pacific concerns the transport by mesoscale eddies, which exhibit pronounced and regionally distinct imprints on O_2 distribution and variability in ocean models (Bettencourt et al., 2015; Frenger et al., 2018; Eddebbar et al., 2021). Tropical instability vortices (TIVs), which are large and fast propagating eddies that are associated with Tropical Instability Waves (TIWs), strongly influence the instantaneous O_2 distribution during their westward propagation (Eddebbar et al., 2021) due to their intense vertical and lateral circulation (Kennan & Flament, 2000). The net effect of eddy transport on O_2 supply and its steady state and seasonal budget balance in the equatorial Pacific, however, have so far not been quantified, and its representation in climate models may contribute to their O_2 biases which persist across model generations (Cabr   et al., 2015; Busecke et al., 2019, 2022). And while diffusive mixing has been recently proposed as a potential source of O_2 at depth in the Atlantic basin (Hahn et al., 2014; Brandt et al., 2015; Calil, 2023) and a key factor for future O_2 projections (Couespel et al., 2019; Portela et al., 2020; L  vy et al., 2022), its net contribution to the O_2 budget and the processes underlying its spatial and temporal variability are poorly known. This is especially of interest in the equatorial Pacific, where the thermocline is shallow and where the high shear (Figure 1d) induced by the EUC and South Equatorial Current (SEC) induces intense turbulent mixing and substantial heat exchange between the thermocline and the surface layer (Moum et al., 2009; Holmes & Thomas, 2015; Cherian et al., 2021; Whitt et al., 2022).

These advective and mixing processes governing O_2 transport in the equatorial Pacific are tightly intertwined across temporal and spatial scales. Shear-driven turbulence along the equatorial cold tongue, for instance, is seasonally modulated by the propagation of TIWs and their eddy structures (Moum et al., 2013; Lien et al., 2008; Holmes & Thomas, 2015; Cherian et al., 2021), which themselves arise from barotropic and baroclinic instabilities generated by the shear between the zonal jets (Willett et al., 2006). These physical interactions may also play key roles in facilitating the vertical supply of nutrients from the EUC to the euphotic layer along the equatorial Pacific, intensifying productivity at the surface (Strutton et al., 2001; Vichi et al., 2008; Strutton et al., 2011; Tian et al., 2018), and potentially modulating O_2 consumption rates in the thermocline. Identifying the contributions and mechanisms by which these transport processes balance O_2 removal in the ocean interior is critical for understanding the observed expansion of the ODZs and predicting their future (Busecke et al., 2022), but has so far been hindered by sparse sampling (Brandt et al., 2015; Ito et al., 2017) and inadequate representation of the equatorial current system and mesoscale eddies in coarse models (Cabré et al., 2015; Busecke et al., 2019).

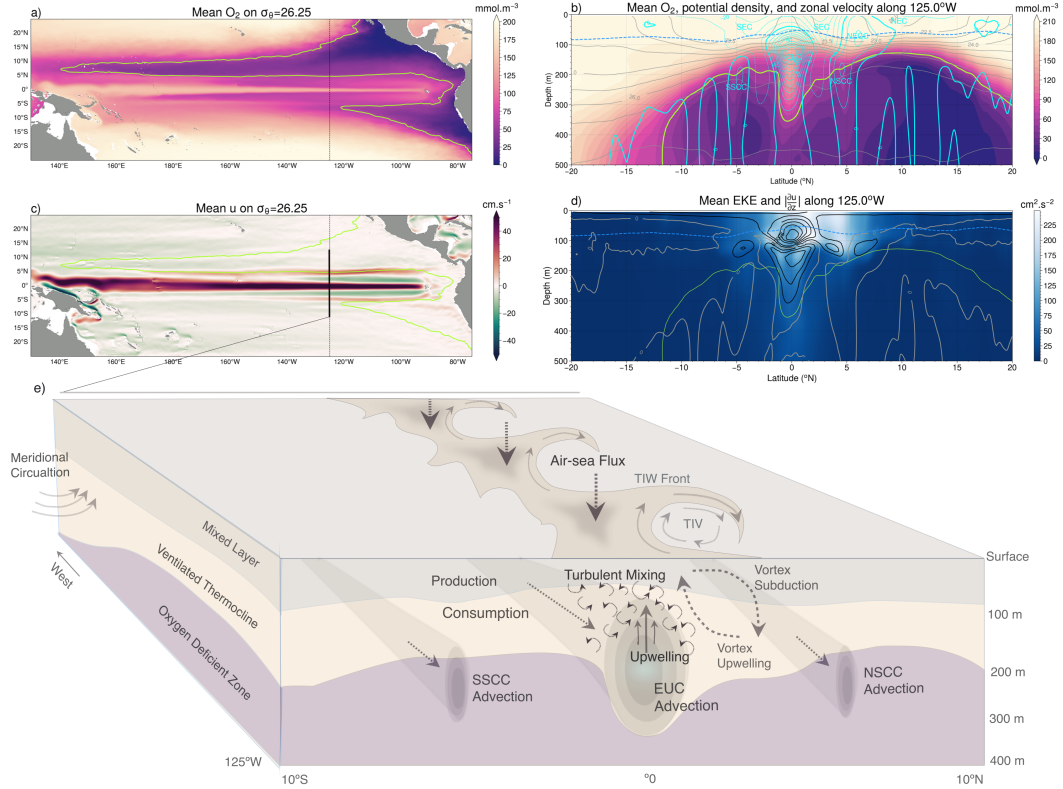


Figure 1. Tropical Pacific O_2 distribution and driving processes. Mean O_2 on the 26.25 isopycnal (a) and along $125^\circ W$ (b) with zonal velocity (cyan) contoured every 10 cm.s^{-1} (bold denotes zero, dashed indicate negative values), potential density (gray), mixed layer depth (dashed blue), and hypoxic boundary (lime) in the CESM simulation. c) Mean eastward zonal velocity on the 26.25 isopycnal. d) Mean eddy kinetic energy (EKE) in shading and the absolute mean vertical shear of the zonal velocity ($|\frac{\partial u}{\partial z}|$) contoured every 0.0025 s^{-1} (gray denotes zero) along $125^\circ W$. The mixed layer depth (dashed blue line) is defined using the maximum buoyancy gradient criteria of Large et al. (1997). e) Key processes driving O_2 supply and removal in the equatorial Pacific.

Here, we evaluate the contribution of advective and mixing processes in the equatorial Pacific O_2 budget balance and its seasonality using an eddy resolving simulation of ocean circulation and biogeochemistry. We focus our regional analysis on key processes governing O_2 supply into the upper (0-300 m) eastern and central equatorial Pacific (east of $160^\circ W$ and equatorward of $7^\circ S$ and $7^\circ N$), a highly energetic region that is thought to be ventilated primarily by the EUC and Tsuchiya jets (Stramma et al., 2010). Given their relatively well studied impacts on the transport of heat in the upper equatorial Pacific, we expect that eddy circulation and turbulent mixing may play similarly critical roles in the supply of O_2 in this region. Section 2 details our modeling and budget analysis framework. Next, we assess the steady state O_2 budget and seasonal variability of O_2 supply in the upper equatorial Pacific in Section 3 and Section 4, respectively. We conclude with an exploration of the mechanisms underlying the eddy-mediated mixing of O_2 in the upper equatorial Pacific thermocline in Section 5, followed by a summary and discussion of our findings in Section 6.

2 Methods

2.1 Ocean Model

We evaluate the contribution of physical and biogeochemical drivers of the mean and seasonal O_2 budget balance and their underlying processes using a 5-year eddy resolving hindcast simulation of the Community Earth System Model (CESM) version 1. In this configuration, the ocean is simulated using the Parallel Ocean Program version 2 (POP2) (Smith et al., 2010) with a grid resolution decreasing from 11 km near the equator to 3 km near the poles, and a vertical resolution increasing across 62 layers from 10 m in the upper 160 m to 250m in the abyss. Mixing is parameterized using the K-profile parameterization (KPP) framework, which represents shear-driven turbulent diffusion via a non-linear function of the local gradient Richardson number (Large et al., 1994). Ocean biogeochemistry is simulated using the Biogeochemical Elemental Cycle (BEC) model (Moore et al., 2013), which simulates lower trophic plankton dynamics, including three phytoplankton functional groups and one zooplankton group, coupled to the biogeochemical cycles of oxygen, carbon, and nutrients (Long et al., 2013).

The hindcast simulation of CESM is forced with a repeating annual climatological cycle of the atmospheric state using the Coordinated Ocean-Ice Reference Experiment (CORE) framework (Large & Yeager, 2004; Griffies et al., 2009). Ocean physical and biogeochemical properties were initialized using interpolated climatological fields from mapped observational products when available, e.g. the World Ocean Circulation Experiment (Gouretski & Koltermann, 2004) for temperature and salinity, and the World Ocean Atlas (WOA) for O_2 and macro-nutrients (Garcia et al., 2005), and when not available using interpolated fields from a previous hindcast CESM simulation integrated at the nominal 1° resolution (Long et al., 2013). The model was spun up for 15 years for physics and one year for biogeochemistry (Harrison et al., 2018), and then integrated forward for 5 years using the CORE atmospheric climatological annual cycle, and outputs were saved at 5 day frequencies. Despite its short duration, this spin up period allows the mesoscale circulation and its imprints on biogeochemical and plankton distributions to develop and stabilize enough while operating on tracer distributions that are similar to the mapped observational products used for initialization (e.g. O_2 and macro-nutrients), and has been recently used to evaluate the impact of eddies across a range of ocean biogeochemical cycles (Harrison et al., 2018; Song et al., 2018; Rohr et al., 2020; Eddebbar et al., 2021).

At the 0.1° resolution, CESM yields an energetic mesoscale eddy field with more realistic winter mixed layers and chlorophyll distributions than the more widely used 1° configuration (Harrison et al., 2018; Rohr et al., 2020), and generally reproduces the broad scale distribution of the eddy-induced correlation between chlorophyll and sea surface

height anomalies observed from satellites (Song et al., 2018). In the equatorial Pacific, ocean circulation and O_2 structure are generally improved at 0.1° vs the 1° solution, with strong seasonality in the zonal flow and meridional shear that gives rise to well resolved TIWs and their chlorophyll imprints (Eddebbar et al., 2021). The 0.1° configuration is also characterized by a less zonally tilted EUC and the emergence of the Tsuchiya jets and yields more realistic O_2 distributions (Eddebbar et al., 2021), in general agreement with recent global and regional model simulations that showcase improved representation of tropical Pacific ocean circulation and O_2 structures at higher resolution (Busecke et al., 2019; Margolskee et al., 2019).

2.2 Oxygen Budget

We assess the contribution of different processes to the O_2 budget balance, calculated in CESM as follow:

$$\frac{\partial O_2}{\partial t} = -\nabla \cdot (\mathbf{u}O_2) + D(O_2) + \frac{\partial}{\partial z} k \frac{\partial O_2}{\partial z} + J(O_2) \quad (1)$$

where $-\nabla \cdot (\mathbf{u}O_2)$ represents the lateral and vertical O_2 advection, $D(O_2)$ and $\frac{\partial}{\partial z} k \frac{\partial O_2}{\partial z}$ represent lateral and vertical diffusive mixing, respectively, and $J(O_2)$ represents the net balance between production of O_2 via photosynthesis and consumption by microbial respiration.

We assess the contribution of different budget terms in steady state by decomposing the advection term into a mean and eddy advective component using a Reynolds decomposition (McGillicuddy Jr et al., 2003) in the time-averaged budget equation as follow:

$$\overline{\frac{\partial O_2}{\partial t}} = -\nabla \cdot (\overline{\mathbf{u}}\overline{O_2}) - \nabla \cdot (\overline{\mathbf{u}'O_2'}) + \overline{D(O_2)} + \overline{\frac{\partial}{\partial z} k \frac{\partial O_2}{\partial z}} + \overline{J(O_2)} \quad (2)$$

where the bar denotes the average of the climatological monthly mean over the 5 year model solution, $-\nabla \cdot (\overline{\mathbf{u}}\overline{O_2})$ represents lateral and vertical O_2 advection by the mean flow, $-\nabla \cdot (\overline{\mathbf{u}'O_2'})$ quantifies the eddy advection effects, $\overline{\frac{\partial}{\partial z} k \frac{\partial O_2}{\partial z}}$ represents the mean contribution of vertical diffusive mixing, and $\overline{J(O_2)}$ represents the balance of mean O_2 production and consumption by photosynthesis and microbial consumption.

The eddy term $(-\nabla \cdot (\overline{\mathbf{u}'O_2'}))$, which quantifies the covariance of the time-deviating anomalies in the O_2 advection divergence, is calculated as the difference of the total and mean advective terms as:

$$-\nabla \cdot (\overline{\mathbf{u}'O_2'}) = -\nabla \cdot (\overline{\mathbf{u}O_2}) + \nabla \cdot (\overline{\mathbf{u}}\overline{O_2}) \quad (3)$$

Our choice of using the 5-day mean deviations from the 5-year climatological monthly mean for the eddy term in the Reynolds decomposition aims at isolating the effects of eddy advection from the large scale mean advective processes (e.g. ECS) as well as their seasonal variability.

The effects of mesoscale eddy lateral mixing is explicitly resolved at this resolution and the parameterized lateral diffusive mixing ($\overline{D(O_2)}$) is negligible compared to other budget terms and is not shown here for brevity. Our analysis of the seasonal cycle in Section 4 is based on seasonally averaging the climatological monthly means for boreal winter using December through February, boreal spring using March through May, boreal summer using June through August, and boreal fall using September through November.

3 The Oxygen Budget Balance in Steady State

We first consider the contribution of different physical and biogeochemical processes to the steady state budget balance and structure of O_2 , shown in Figure 2 as zonal averages over the eastern and central equatorial Pacific (80°W - 160°W). This region is characterized by enriched O_2 values in the mixed layer due to intense air-sea gas exchange and photosynthetic production of O_2 , overlaying a shallow oxycline that bounds the northern and southern tropical Pacific ODZs (Figure 2a). This complex subsurface structure is set by a net balance of large and often opposing contributions from transport and biological processes (Figure 2 and Figure S1 in Supporting Information). Microbial consumption is a major sink of O_2 throughout the equatorial Pacific thermocline, with intensified consumption centered around 5°S and 5°N , reflecting the divergence of sinking organic carbon away from its equatorial source of production via Ekman divergence and the tropical cells (Figure 2d). This O_2 removal is largely replenished by vigorous vertical mixing in the upper thermocline ($50\text{--}150\text{ m}$, $23.5 < \sigma_\theta < 25.5\text{ kg m}^{-3}$), though advection plays a more dominant role in supplying O_2 deeper in the thermocline ($> 150\text{ m}$, $\sigma_\theta > 25.5\text{ kg m}^{-3}$) and particularly near the ODZ boundaries (Figure 2b).

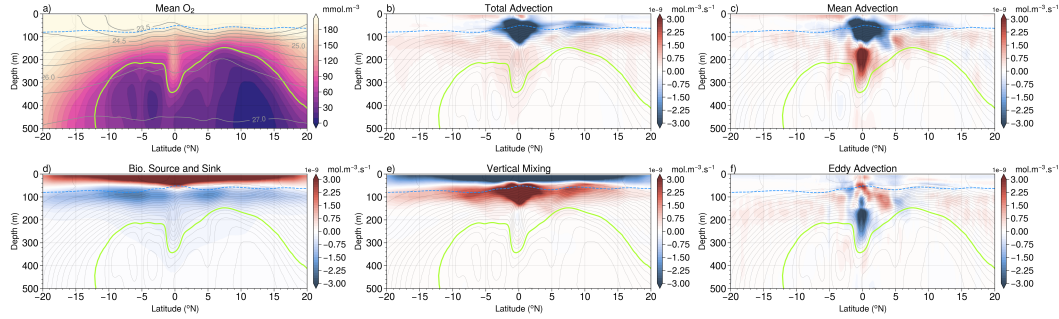


Figure 2. Mean O_2 budget decomposition zonally averaged over the eastern and central equatorial Pacific (80°W - 160°W) in the upper 500 m in CESM, including a) mean O_2 concentrations and potential density (gray contours), and contributions of b) total advection, c) mean advection, d) biological sources and sinks, e) vertical mixing, and f) eddy advection to the steady state O_2 budget balance. Positive values in b-f) denote positive contribution to the O_2 budget balance. Dashed blue line outline the mixed layer depth, grey contours in b-f) outline mean O_2 concentrations contoured every 10 mmol.m^{-3} , and the hypoxic boundary is shown in neon.

The contribution of advection shown in Figure 2b reflects both i) a “mean” component associated with large scale upwelling and lateral flow by the ECS and the shallow overturning circulation, and ii) an “eddy” component associated with the westward propagation of TIWs and their vortex structures (i.e. TIVs) which dominate eddy kinetic energy (EKE) in this region (Ubelmann & Fu, 2011), as well as meanderings and instabilities generated along the EUC path at depth. A decomposition of these mean and eddy terms (Figure 2b-c and 2f) shows that mean advection acts both to i) substantially reduce O_2 levels below and within the surface mixed layer between 2°S and 5°N via the large scale upwelling of low- O_2 thermocline waters to the surface (Figure S1f and S1i in Supporting Information), and ii) supply O_2 to the eastern basin west of 160°W through the zonal and meridional flow of waters (Figure S1d-e and S1g-h in Supporting Information). The lateral supply of O_2 from the western part of the equatorial Pacific basin to the east is driven largely by the EUC, which transports about $4.66 \times 10^6\text{ mol s}^{-1}$ of oxygen across 160°W from the base of the mixed layer through $\sigma_\theta=26.5\text{ kg m}^{-3}$. This zonal EUC transport is further supplemented poleward of 4°N and 4°S by the Tsuchiya Jets which together advect about $0.41 \times 10^6\text{ mol s}^{-1}$ of oxygen across 160°W , and the

convergence of ventilated waters by the tropical and subtropical cells which advect a net equatorward flux of $1.95 \times 10^6 \text{ mol s}^{-1}$ of oxygen across 7°S and 7°N from the base of the mixed layer through $\sigma_\theta = 26.5 \text{ kg m}^{-3}$ (Figure S1d-e and S1g-h in Supporting Information).

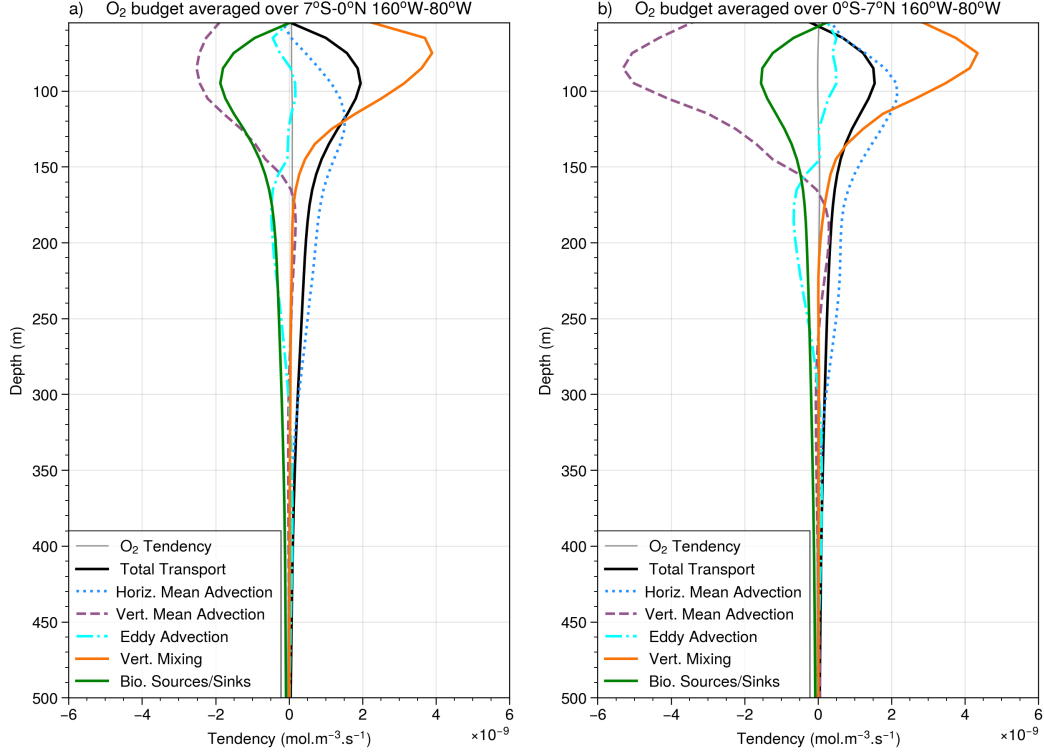


Figure 3. Mean O_2 budget decomposition laterally averaged over a) the southern (7°S - 0°) and b) northern (0° - 7°N) central and eastern (80°W - 160°W) equatorial Pacific in CESM. Total transport (black line) includes contributions from mean and eddy advection as well as vertical mixing, while biological sources and sinks (green line) represents the balance of O_2 production by photosynthesis and consumption by respiration.

Compared to mean advection and vertical mixing, the eddy advection term contributes modestly to supply O_2 below the mixed layer from 0° - 5°N (Figure 2f and Figure 3b), acting to counteract the negative contribution by the mean upwelling in this region and depth range (50 – 150 m). The positive eddy-driven flux of O_2 into the upper northern equatorial thermocline reflects the integrated effects of transient eddy stirring and downwelling of oxygenated waters by TIVs in this region (Eddebbbar et al., 2021). The role of eddy advection, however, is smaller south of the equator (Figure 2f and Figure 3a) where EKE activity is much weaker (Figure 1d) and less structured (Ubelmann & Fu, 2011). Deeper in the equatorial Pacific thermocline (150-300 m), eddy advection contributes negatively along the equator (2°S - 2°N) to the O_2 budget as the meandering of the EUC and instabilities generated along its path recirculate and stir low- O_2 waters from the neighboring ODZs into the equatorial oxygenated tongue, counteracting the positive contribution by the mean zonal advective supply (Figure 2f and Figure 3). Away from the equator (poleward of 7°N and 7°S), Figure 2f shows that eddies contribute broadly to supply O_2 throughout the oxycline (100-200 m), as similarly found in an O_2 budget study of the Atlantic basin (Calil, 2023).

The critical role of vertical mixing in sustaining O_2 supply in the upper equatorial Pacific thermocline is further illustrated in Figure 3, which shows the vertical profile of the contribution of the budget terms averaged over the southern (7°S - 0°) and northern (0° - 7°N) central and eastern equatorial Pacific. We set our meridional averaging boundaries at 7°S and 7°N to capture the full contribution of eddies and off-equatorial zonal circulation by TIVs and the Tsuchiya jets, respectively. Vertical mixing dominates the O_2 supply from about 50 m to about 120 m below, and remains an important component of the net transport of O_2 down to 150 m depth below which lateral advection becomes the main supply pathway into the eastern and central equatorial Pacific (Figure 3). The pattern of vertical mixing driving O_2 supply in the upper water column and lateral advection dominating at depth is relatively consistent between the eastern and central parts of the equatorial Pacific basin (Figure 2 and Figure S2 in Supporting Information). Some differences between the two regions, however, arise with mixing playing a meridionally more expansive role in the eastern Pacific where the oxycline is shallower (Figure S2d and S2h) while eddy and mean zonal advection play more pronounced roles in the central Pacific (Figure S2b-c and S2f-g) where EKE and the EUC are intensified, respectively.

The outsized role of mixing in the upper equatorial Pacific O_2 budget balance can be attributed to the superposition of i) the pronounced vertical gradient in O_2 set by equatorial upwelling, and ii) the high diffusivity set by the dynamically unique nature of the flow regime along the equatorial Pacific. Within a couple degrees of the equator above the EUC, the high vertical shear between the opposing EUC and SEC (Figure 1d) sustains a marginally stable flow state in the upper ocean characterized by intermittent but strong eddy-mediated turbulent mixing below the base of mixed layer that drives intense heat uptake into the ocean's interior (Moum et al., 2009; Holmes et al., 2019; Cherian et al., 2021; Deppenmeier et al., 2022; Whitt et al., 2022). The spatial extent of the vertical mixing of O_2 shown in Figure 2e is generally similar to previously reported spatial patterns of vertical mixing of heat (Holmes et al., 2019; Deppenmeier et al., 2022; Whitt et al., 2022), with enhanced contributions below the mixed layer (50-150 m) along the cold tongue, and weaker contributions away from the equator associated with turbulent mixing and TIVs (Cherian et al., 2021). A similar role for equatorial turbulence is thus shown here for driving intense local transport of O_2 into the upper thermocline that supplements the advective transport of remotely ventilated waters via the mean zonal and meridional circulation at depth.

4 Seasonal Drivers of Oxygen Supply

The lateral advective and vertical mixing processes driving the renewal and budget balance of O_2 in the equatorial Pacific described in Section 3 are strongly seasonal. Figure 4 shows the seasonal mean O_2 flux from the main supply sources of O_2 into the eastern and central equatorial Pacific thermocline, namely the vertical turbulent mixing flux of O_2 across the mixed layer base integrated over the 7°N - 7°S and 160°W - 80°S area, and the lateral advective fluxes including the mean zonal advective flux across 160°W and the mean equatorward meridional advective flux of O_2 across 7°N and 7°S integrated from the base of the mixed layer base through $\sigma_\theta=26.5 \text{ kg m}^{-3}$. In the analysis of the seasonal variability and mechanisms underlying the vertical mixing flux of O_2 , we focus from here onward on the local mixing flux as parameterized in the KPP scheme (Large et al., 1994), and leave out contributions from the non-local KPP transport term which plays a negligible role in the equatorial Pacific and is thus left out of this discussion for clarity and brevity. Although the total transport of O_2 (gray bar in Figure 4a) varies modestly across seasons (e.g. 46% increase from boreal winter to summer), the individual fluxes comprising this transport vary substantially (~ 160 - 180% change between seasons) and out of phase. During the spring months when vertical mixing and meridional advective fluxes are weak, O_2 supply is dominated by zonal advection (blue in Figure

3a), which sustains a seasonal mean flux of $\sim 5 \times 10^6 \text{ mol s}^{-1}$ primarily via the eastward EUC transport of remotely ventilated waters. Following spring, the downward turbulent mixing of O_2 increases nearly threefold to $\sim 4.5 \times 10^6 \text{ mol s}^{-1}$ during summer and becomes a leading source of O_2 supply in fall (yellow in Figure 4a), contributing substantially to balance the increase in microbial consumption and upwelling during these months (Figure S3 in Supporting Information). Despite their overall weaker magnitudes in winter, mixing and advective fluxes contribute nearly equally during this season, thus sustaining a relatively stable net supply of O_2 year-round in this region (Figure 4a).

The large seasonality of O_2 supply from each of these different pathways is driven mainly by their unique dynamical responses to the annual cycle in the overlying winds. Figure 4c shows the total meridional flux of O_2 (brown line), separated into its northern (dark green) and southern (light green) components, and reveals a strong seasonality in these fluxes that is linked to the variability in the equatorial zonal wind stress (dashed blue line), with increased equatorward transport from late summer through winter when the wind stress is strong, and reduced transport from spring through mid-summer when the wind stress is weak. This seasonal relationship likely reflects the northward migration of the southeasterly winds across the equator during fall and summer, and the subsequent impacts of reduced equatorial wind stress on Ekman surface divergence and the equatorward return flow in the thermocline (Johnson & McPhaden, 1999; Lee & Fukumori, 2003), though changes in wind stress away from the equator may also play a role (Graffino et al., 2019).

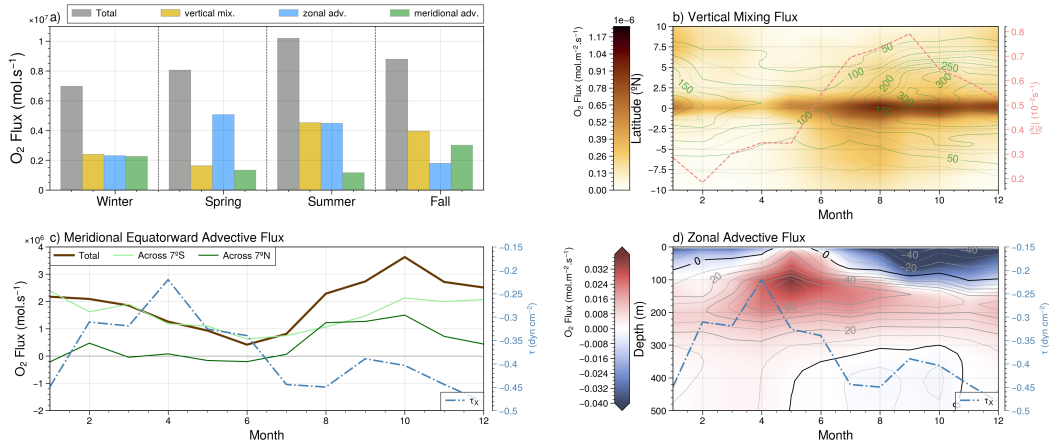


Figure 4. Seasonal drivers of O_2 supply in the upper equatorial Pacific in CESM. a) Seasonal mean fluxes due to vertical mixing (yellow) across the base of the mixed layer integrated over 7°S - 7°N and 80°W - 160°W , zonal advection across 160°W (blue) integrated over 7°S - 7°N from the base of the mixed layer through $\sigma_\theta=26.5 \text{ kg m}^{-3}$, and meridional advection across 7°S and 7°N (green) integrated over 80°W - 160°W from the base of the mixed layer through $\sigma_\theta=26.5 \text{ kg m}^{-3}$, and the sum (grey). b) Hovmöller plot of climatological monthly mean O_2 vertical mixing flux across the mixed layer base averaged zonally over 80°W - 160°W , along with surface EKE ($\text{cm}^2 \text{ s}^{-2}$) in green and $|\frac{\partial u}{\partial z}|$, the absolute vertical shear of zonal velocity averaged over the high shear depth range (80-120 m) from 2°S - 2°N (light red). c) Climatological monthly mean meridional equatorward O_2 flux across 7°S and 7°N , along with equatorial (2°S - 2°N) zonal wind stress (dashed blue) averaged over 80°W - 160°W . Panel d) shows the climatological monthly mean eastward zonal flux of O_2 across 160°W averaged over 7°S to 7°N , along with the equatorial zonal wind stress (dashed blue).

From late winter and through early summer, an intensification and shoaling of the eastward flow by the EUC drives larger zonal fluxes of O_2 into the central and eastern Pacific with corresponding reductions in the magnitude of equatorial wind stress (Figure 4d). This is followed during late summer through early winter by a major slowdown of this zonal supply of O_2 as wind stress intensifies along the equator. This seasonal coupling of the EUC transport to wind forcing (Figure 4d) is likely driven by a complex interaction of zonal wind stress impacts on the zonal pressure gradient, momentum budget, and propagation of Kelvin waves in the equatorial Pacific (Johnson et al., 2002; Kessler, 2006; Sen Gupta et al., 2012).

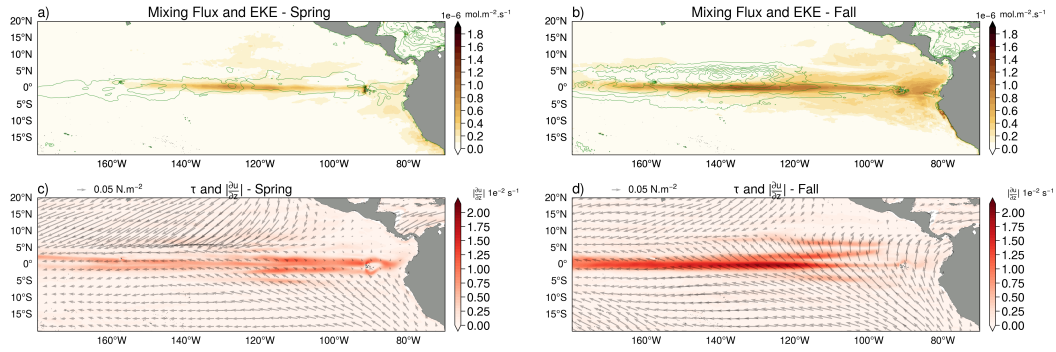


Figure 5. Seasonal mean O_2 flux across the base of the mixed layer due to local vertical mixing along with EKE contoured (green) every $100 \text{ cm}^2 \text{ s}^{-2}$ for a) boreal spring and b) boreal fall in the CESM simulation. Lower panels show the surface wind stress and $|\frac{\partial u}{\partial z}|$, the absolute vertical shear of zonal velocity averaged over the high shear depth range (80-120 m) from 2°S - 2°N , for c) boreal spring and d) boreal fall. The O_2 mixing flux shown in a) and b) represents the maximum value of the local vertical mixing flux below the mixed layer depth (typically 80-120 m). The mixed layer depth is defined in CESM using the buoyancy gradient criteria of Large et al. (1997).

A major consequence of the seasonal cycle in wind forcing is its modulation of the vertical shear in zonal velocity, particularly along the equator where the flow is marginally stable. Figure 4b and Figure 5 detail the latitudinal and seasonal characteristics of the vertical mixing flux of O_2 , which intensifies along the 2°S - 2°N band during summer and fall when the vertical shear of the zonal velocity (dashed red line in Figure 4b and red shading in Figure 5c-d) is highest, and declines substantially during spring when the shear is low. The seasonal and spatial intensity of the vertical mixing flux of O_2 along the equator also co-vary with EKE (green contours in Figure 4b and 5a-b), which increases in summer and fall through the generation and propagation of TIWs and their vortices and reaches its minima in spring when TIWs are typically absent. The seasonal wind forcing of the vertical and lateral shear between the equatorial currents influences both the turbulent mixing in the high shear region (80-120 m) of the EUC as well as the generation of barotropic and baroclinic instabilities in the zonal flow that develop into TIWs, which in turn can influence turbulent mixing (Holmes & Thomas, 2015). This seasonal co-variability of vertical mixing of O_2 with the vertical shear and EKE likely reflects more nuanced and complex interactions across scales, which we explore in the following section.

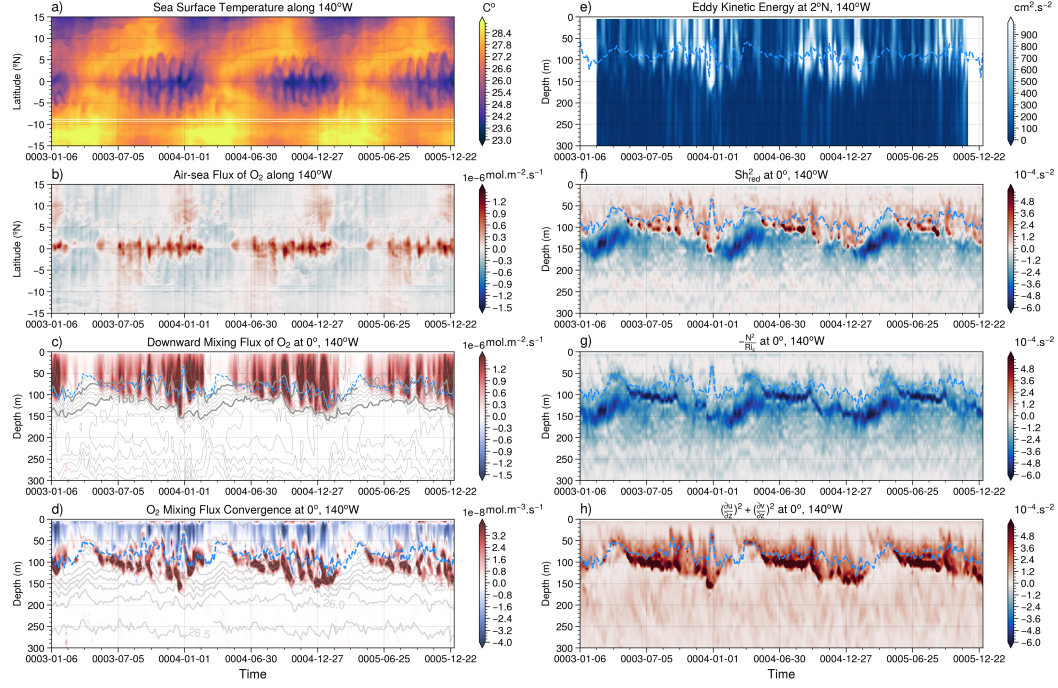


Figure 6. Processes driving TIW modulation of equatorial Pacific O_2 mixing at $140^\circ W$ in CESM. a) Hovmöller plot of a) SST, b) air-sea flux of O_2 , c) downward local mixing flux of O_2 (shading) and O_2 values (grey contours), and d) O_2 local mixing flux convergence (shading) and density layers (grey contours). e) EKE at $2^\circ N$, $140^\circ W$, f) Reduced shear squared, g) Buoyancy frequency scaled by the critical Richardson number, and h) squared vertical shear of the lateral velocity field. Dashed blue line in c) through h) outline the mixed layer depth.

5 Mechanism of Eddy-Mediated Turbulent Mixing of Oxygen

Given its substantial influence on the mean state budget balance and seasonal variability of O_2 supply in the upper equatorial Pacific thermocline, we further examine the underlying drivers of the temporal and spatial structure and variability of vertical mixing of O_2 and its interaction with mesoscale activity in CESM. Figure 6 elucidates the link between the vertical mixing of O_2 and mesoscale activity during the last three years of the CESM simulation at $140^\circ W$ along the equator, a site where shear-driven turbulence and its modulation by eddy dynamics have long been observed and simulated (Chereskin et al., 1986; Halpern et al., 1988; Lien et al., 2008; Moum et al., 2009, 2013; Inoue et al., 2012, 2019; Holmes & Thomas, 2015; Cherian et al., 2021; Whitt et al., 2022). The seasonal intensification of the O_2 mixing flux does not covary with the seasonal shoaling and deepening of the oxycline (Figure 6c), but instead occurs intermittently from summer through mid-winter and coincides with TIW events, outlined by their cold wave-like imprints on SSTs and deep reaching patches of high EKE (Figure 6a, 6c and 6e), while spring showcases little eddy activity or mixing of O_2 . The arrival of TIWs at $140^\circ W$ during summer and fall induces intense surface air-sea fluxes of O_2 near the equator and enhanced downward mixing fluxes of O_2 that penetrate well below the mixed layer down to 150 m depth (Figure 6a-c). The uptake of O_2 due to enhanced mixing is likely buffered though only slightly by thermodynamic effects as TIWs induce an intense air-to-sea flux of heat (Cherian et al., 2021) and a subsequent outgassing of O_2 , similar to ENSO-driven variability in air-sea O_2 flux (Eddebbar et al., 2017). Figure 6d shows that the convergence of this vertical mixing acts to increase O_2 below the mixed layer and throughout the up-

per thermocline ($23.5 < \sigma_\theta < 25.5 \text{ kg.m}^{-3}$). As shown by the logarithmic distribution of the shear-driven turbulent flux of O_2 (Figure S4 in Supporting Information), these intermittent high-shear TIW-mediated mixing events have a considerable influence on setting the mean state of the O_2 vertical mixing and total transport in the upper equatorial Pacific.

The tight link between eddy activity and downward turbulent mixing of O_2 in the equatorial Pacific can be understood in the context of TIW modulation of equatorial turbulence as parameterized in CESM. The upper equatorial Pacific is typically in a state of marginal stability due to the high vertical shear induced by the EUC and SEC, with shear turbulence arising when the vertical shear of lateral velocities prevail over the stabilizing effects of stratification (Smyth & Moum, 2013; Moum, 2021). This subgrid scale turbulence is parameterized as a local shear-driven diffusivity (K_S) in the KPP scheme through a function of the gradient Richardson Number (Ri_g) as follows (Large et al., 1994; Smith et al., 2010):

$$K_S = \begin{cases} K_0, & \text{if } Ri_g < 0 \\ K_0 \left[1 - \left(\frac{Ri_g}{Ri_c} \right)^2 \right]^3, & \text{if } 0 < Ri_g < Ri_c \\ 0, & \text{if } Ri_g > Ri_c \end{cases} \quad (4)$$

where $K_0 = 50 \times 10^{-4} \text{ m}^2 \cdot \text{s}^{-1}$, and Ri_g is calculated as:

$$Ri_g = \frac{N^2}{\left(\frac{\partial u}{\partial z} \right)^2 + \left(\frac{\partial v}{\partial z} \right)^2} \quad (5)$$

where $N^2 = \frac{\partial b}{\partial z}$ is the buoyancy frequency squared, $b = -\frac{g\rho}{\rho_0}$ is the buoyancy, and $\left(\frac{\partial u}{\partial z} \right)^2 + \left(\frac{\partial v}{\partial z} \right)^2$ is the sum of the squared shears in zonal and meridional velocities. Ri_c refers to a critical Ri threshold, set here at 0.8, a value that most consistently yields the diffusive mixing from resolved turbulence in the equatorial regime in Large Eddy Simulation (LES) experiments (Large & Gent, 1999). When the Ri_g falls below Ri_c , shear instabilities develop and K_S steeply increases towards the maximum value of K_0 . When Ri_g values exceed Ri_c , shear instabilities are inactive and K_S is set to 0. A key metric for quantifying the contribution of changes in stratification vs vertical shear in inducing turbulence is the reduced shear squared (Sh_{red}), calculated as:

$$Sh_{red}^2 = \left(\frac{\partial u}{\partial z} \right)^2 + \left(\frac{\partial v}{\partial z} \right)^2 - \frac{N^2}{Ri_c} \quad (6)$$

where N^2 is normalized by Ri_c following Cherian et al. (2021) and acts to stabilize the flow, while $\left(\frac{\partial u}{\partial z} \right)^2 + \left(\frac{\partial v}{\partial z} \right)^2$ acts to destabilize it. Positive values of Sh_{red} indicate periods when the flow is turbulent ($Ri_g < Ri_c$), and are outlined in Figure 6f as intense positive (red) patches (Figure 6f) where variations in the vertical shear in lateral velocities overcome the stratification effects (Figure 6g-h). These marked increases in the vertical shear are tightly coupled to the intensification of EKE via the westward passage of TIWs (Figure 6e-h) and their vortex stretching effects (Holmes & Thomas, 2015; Inoue et al., 2019), which push the flow state towards instability. As TIWs propagate westward through 140°W , K_S increases rapidly and combined with the pronounced vertical gradient of O_2 in the upper thermocline, the downward mixing flux of O_2 is significantly intensified (Figure 6). The reduction of EKE when TIWs are largely inactive (e.g. during spring) and the subsequent weakening of the vertical shear bring the flow back towards a stable state ($Ri_g > Ri_c$), substantially weakening the vertical diffusive flux of O_2 during such periods (Figure 6).

We further illustrate the spatial structure of how TIWs impacts the downward turbulent mixing of O_2 in Figure 7, which shows a 5-day mean snapshot of the air-sea flux,

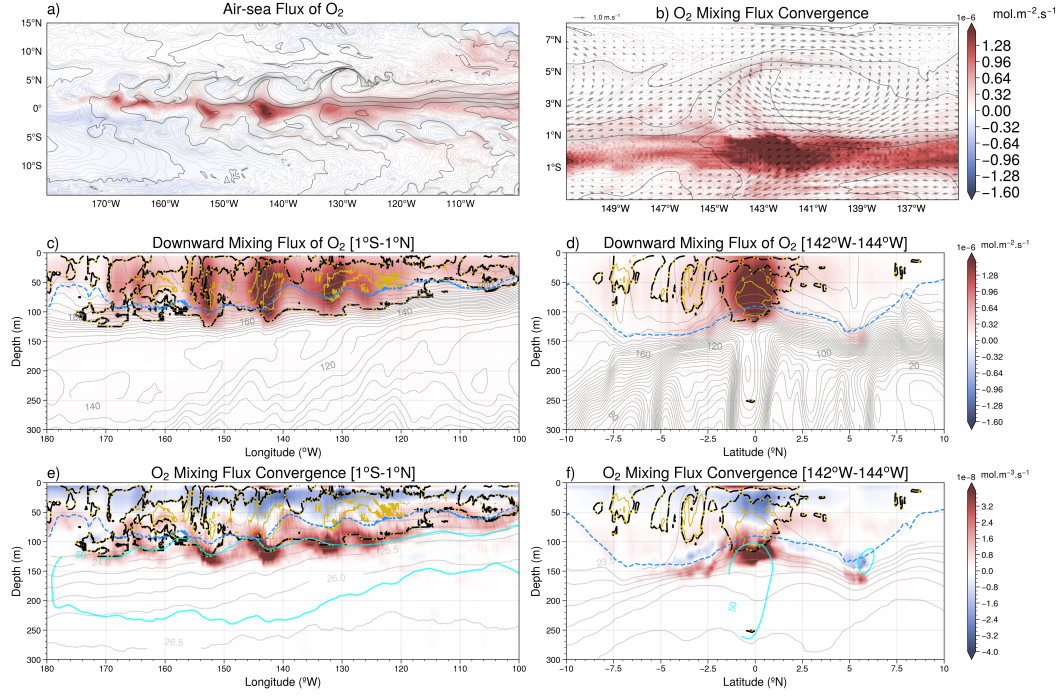


Figure 7. Eddy-Mediated Mixing of Oxygen. 5-day mean values around October 3, of year 5 of the CESM simulation of a) air-sea flux of O_2 and SST (contoured every 1° in bold and 0.1 in light), b) local mixing flux convergence integrated from the base of the mixed layer through the 26.5 isopycnal and horizontal velocity at 50 m depth zoomed on a TIW centered around $143^\circ W$. Panels c) and d) show the downward local mixing flux of O_2 averaged over $1^\circ S$ - $1^\circ N$ and $142^\circ W$ - $144^\circ W$ (color shading), respectively, along with the low Ri layer contoured at the critical value in POP2 at 0.8 (dashed black and yellow) and 0.4 (yellow), mixed layer in dashed blue, and O_2 contours in light gray. Panels e) and f) show the O_2 local mixing flux convergence averaged over $1^\circ S$ - $1^\circ N$ and $142^\circ W$ - $144^\circ W$ (color shading), respectively, along with the low Ri layer (dashed black and yellow), isopycnals (gray contours), mixed layer (dashed blue), and the 50 cm s^{-1} zonal velocity contour outlining the EUC region of high shear (cyan).

local vertical mixing flux, and the convergence of the vertical mixing flux of O_2 during a period when TIWs were active. Intense patches of air-sea flux and downward mixing flux are co-located with the cold cores of TIWs along the equator (Figure 7a-d). Below the surface, turbulent regions outlined by Ri_c contours (black and yellow) coincide with these cores throughout the upper 120m between $2^\circ S$ and $2^\circ N$, and showcase an intense mixing flux of O_2 and maxima in the vertical convergence of this flux that reach well below the mixed layer and into the core of the EUC (Figure 7e-f). Figure 6 and 7 thus suggest that mesoscale eddies sustain a fast and intense vertical pathway of O_2 exchange from the surface to the thermocline via the TIW modulation of shear instability. The integrated effects of this intermittent TIW-mediated mixing of O_2 leads to a substantial injection of O_2 over the eddy lifetimes with considerable influence on the steady state and seasonal O_2 budget balance (Figures 2-4).

6 Summary and Discussion

Our eddy-resolving model analysis of the equatorial Pacific O_2 budget reveals that turbulent mixing and its modulation by mesoscale eddies play a critical role in supplying O_2 to the upper (50-150 m) thermocline. This O_2 supply acts to augment the previously reported replenishment of O_2 by the EUC, Tsuchiya jets, and meridional circulation deeper (150-300 m) in the thermocline (Stramma et al., 2010; Busecke et al., 2019; Margolskee et al., 2019; Duteil et al., 2014), and suggests that both advective and mixing processes and their interplay sustain the ventilation of the equatorial Pacific thermocline and the presence of the equatorial oxygenated tongue separating the tropical Pacific ODZs. Our Reynolds decomposition further shows that mesoscale eddies play a spatially complex but relatively minor direct role through their eddy advection effects in the equatorial Pacific O_2 budget balance, supplying O_2 along the high EKE region of the upper equatorial Pacific (down to 150 m) and reducing O_2 along the EUC path at depth (150-300 m). These mixing and advective sources of O_2 are highly seasonal and are driven by the annual cycle in surface wind forcing which i) modulates the magnitude of lateral advection of remotely ventilated waters into the central and eastern equatorial Pacific, and ii) controls the seasonality in EKE and vertical shear of the zonal flow that drives the local downward mixing of O_2 . We further examine the processes underlying the vertical mixing of O_2 and its relationship to eddy activity, and find that TIWs strongly modulate the turbulent flux of O_2 via their eddy impact on the vertical shear in lateral velocities. Thus, while eddies play a relatively minor role in the equatorial Pacific O_2 budget balance through their direct eddy advection effects, they play a large indirect role in supplying O_2 into the upper thermocline via their modulation of equatorial shear instability, which sustains a local ventilation pathway of O_2 from the surface layer to the ocean's interior.

These interactions across processes and scales - from basin-wide currents and mesoscale eddies to fine scale turbulence - underscore the complexity by which past and future changes in the equatorial Pacific O_2 content must be approached. These changes should reflect not only the temperature dependence of gas solubility and changes in remote ventilation via the equatorial current system, but also how local ventilation via turbulent mixing and its modulation by eddies will shift as the tropical Pacific ocean responds to anthropogenic radiative forcing (Vecchi et al., 2006; Ying et al., 2022). Our results also have implications for identifying the source of the underestimate in the interannual variability and long-term trends of O_2 in climate models (Oschlies et al., 2018), where eddies and their impacts on turbulence are not resolved. Finally, the shear-driven downward turbulent flux of heat and O_2 along the equatorial Pacific cold tongue suggests the existence of a positive relationship between air-sea O_2 and heat fluxes. This positive coupling stands in contrast to their well-established negative relationship over most of the world ocean from seasonal to multi-decadal timescales (Garcia & Keeling, 2001; Bopp et al., 2002; Keeling & Garcia, 2002; Keeling et al., 2010; Ito et al., 2017), and suggests that heat uptake can co-occur with increased O_2 in the equatorial Pacific thermocline.

An important caveat underlying our model-based analysis is that turbulent mixing is parameterized in our model, and that the magnitude of this term and its impacts on tracer transport away from the equator and $140^\circ W$ is not well known. A study by Zaron and Moum (2009) further suggests that KPP may overestimate the magnitude of mixing by shear instability in the equatorial region, potentially overestimating the downward turbulent flux of heat in CESM (Deppenmeier et al., 2022), and other important tracers (e.g. O_2). Additionally, our model doesn't resolve or parameterize other sources of mixing stemming from mesoscale circulation, e.g. the cascade of TIW-induced internal lee waves to turbulence (Tanaka et al., 2015), which may have relevant consequences for mixing further down the thermocline near the ODZ boundaries. Future simulations using different mixing schemes along with comparison across models of finer resolution, including higher resolution regional simulations of the equatorial Pacific and Large Eddy

486 Simulations with biogeochemistry, will be key to quantify the sensitivity of our results
 487 to model choice, parameterization scheme, and model resolution. Most importantly, sus-
 488 tained fine scale observations of mixing and biogeochemical tracers such as O_2 along the
 489 equator are needed to quantify the intensity and spatial structure of mixing and its im-
 490 pacts on O_2 variability from diurnal to multi-annual timescales in this region.

491 Nevertheless, the interplay of eddy activity and parameterized shear-driven mix-
 492 ing permitted by the high resolution grid employed in this configuration of CESM presents
 493 new insights into interactions of ocean dynamics and biogeochemistry. The role of eddy-
 494 mediated mixing in driving downward transport of heat and O_2 may have analogous but
 495 inverse impacts on the upward transport of nutrients and carbon from the EUC to the
 496 surface layer, with potentially important implications for modulating the outgassing of
 497 carbon and productivity in this region. Dedicated physical-biogeochemical field campaigns
 498 and enhanced biogeochemical observations targeting TIWs phenomena are particularly
 499 needed to test these model-based findings in nature.

500 **7 Open Research**

501 The CESM model code is publicly available at <https://www.cesm.ucar.edu/models>.
 502 Processed model outputs and analysis code used to complete this work are available on
 503 Zenodo at doi.org/10.5281/zenodo.8371745 and doi.org/10.5281/zenodo.8339521.

504 **Acknowledgments**

505 The authors acknowledge support from the National Science Foundation OCE grant num-
 506 ber 1948599 and high-performance computing support from Cheyenne provided by NCAR's
 507 Computational and Information Systems Laboratory, sponsored by NSF. DBW acknowl-
 508 edges support from the NASA Physical Oceanography and Salinity Science programs and
 509 NASA award NIP20-0113.

References

- Bettencourt, J. H., López, C., Hernández-García, E., Montes, I., Sudre, J., Dewitte, B., ... Garçon, V. (2015). Boundaries of the peruvian oxygen minimum zone shaped by coherent mesoscale dynamics. *Nature Geoscience*, 8(12), 937.
- Bopp, L., Le Quéré, C., Heimann, M., Manning, A. C., & Monfray, P. (2002). Climate-induced oceanic oxygen fluxes: Implications for the contemporary carbon budget. *Global Biogeochemical Cycles*, 16(2), 6–1.
- Brandt, P., Bange, H. W., Banyte, D., Dengler, M., Didwischus, S.-H., Fischer, T., ... Visbeck, M. (2015). On the role of circulation and mixing in the ventilation of oxygen minimum zones with a focus on the eastern tropical north atlantic. *Biogeosciences (BG)*, 12, 489–512.
- Brandt, P., Hahn, J., Schmidtke, S., Tuchen, F. P., Kopte, R., Kiko, R., ... Dengler, M. (2021). Atlantic equatorial undercurrent intensification counteracts warming-induced deoxygenation. *Nature Geoscience*, 14(5), 278–282.
- Busecke, J. J., Resplandy, L., Ditzovsky, S. J., & John, J. G. (2022). Diverging fates of the pacific ocean oxygen minimum zone and its core in a warming world. *AGU Advances*, 3(6), e2021AV000470.
- Busecke, J. J., Resplandy, L., & Dunne, J. P. (2019). The equatorial undercurrent and the oxygen minimum zone in the pacific. *Geophysical Research Letters*, 46(12), 6716–6725.
- Cabré, A., Marinov, I., Bernardello, R., & Bianchi, D. (2015). Oxygen minimum zones in the tropical pacific across cmip5 models: mean state differences and climate change trends. *Biogeosciences*, 12(18), 5429–5454.
- Calil, P. H. (2023). High-resolution, basin-scale simulations reveal the impact of intermediate zonal jets on the atlantic oxygen minimum zones. *Journal of Advances in Modeling Earth Systems*, 15(2), e2022MS003158.
- Chereskin, T., Moum, J. N., Staben, P., Caldwell, D. R., Paulson, C., Regier, L., & Halpern, D. (1986). Fine-scale variability at 140° w in the equatorial pacific. *Journal of Geophysical Research: Oceans*, 91(C11), 12887–12897.
- Cherian, D., Whitt, D., Holmes, R., Lien, R.-C., Bachman, S., & Large, W. (2021). Off-equatorial deep-cycle turbulence forced by tropical instability waves in the equatorial pacific. *Journal of Physical Oceanography*, 51(5), 1575–1593.
- Couespel, D., Lévy, M., & Bopp, L. (2019). Major contribution of reduced upper ocean oxygen mixing to global ocean deoxygenation in an earth system model. *Geophysical Research Letters*, 46(21), 12239–12249.
- Deppenmeier, A.-L., Bryan, F. O., Kessler, W. S., & Thompson, L. (2022). Diabatic upwelling in the tropical pacific: Seasonal and subseasonal variability. *Journal of Physical Oceanography*, 52(11), 2657–2668.
- Drenkard, E. J., & Karnauskas, K. B. (2014). Strengthening of the pacific equatorial undercurrent in the soda reanalysis: Mechanisms, ocean dynamics, and implications. *Journal of Climate*, 27(6), 2405–2416.
- Duteil, O., Böning, C. W., & Oschlies, A. (2014). Variability in subtropical-tropical cells drives oxygen levels in the tropical pacific ocean. *Geophysical Research Letters*, 41(24), 8926–8934.
- Eddebbar, Y., Long, M. C., Resplandy, L., Rödenbeck, C., Rodgers, K. B., Manizza, M., & Keeling, R. F. (2017). Impacts of enso on air-sea oxygen exchange: Observations and mechanisms. *Global Biogeochemical Cycles*, 31(5), 901–921.
- Eddebbar, Y., Subramanian, A., Whitt, D., Long, M., Verdy, A., Mazloff, M., & Merrifield, M. (2021). Seasonal modulation of dissolved oxygen in the equatorial pacific by tropical instability vortices. *Journal of Geophysical Research: Oceans*, 126(11), e2021JC017567.
- Frenger, I., Bianchi, D., Stührenberg, C., Oschlies, A., Dunne, J., Deutsch, C., ... Schütte, F. (2018). Biogeochemical role of subsurface coherent eddies in the ocean: Tracer cannonballs, hypoxic storms, and microbial stewpots? *Global Biogeochemical Cycles*, 32(2), 226–249.

- Gallo, N., & Levin, L. (2016). Fish ecology and evolution in the world's oxygen minimum zones and implications of ocean deoxygenation. In *Advances in marine biology* (Vol. 74, pp. 117–198). Elsevier.
- Garcia, H. E., Boyer, T. P., Levitus, S., Locarnini, R. A., & Antonov, J. (2005). On the variability of dissolved oxygen and apparent oxygen utilization content for the upper world ocean: 1955 to 1998. *Geophysical Research Letters*, 32(9).
- Garcia, H. E., & Keeling, R. F. (2001). On the global oxygen anomaly and air-sea flux. *Journal of Geophysical Research: Oceans*, 106(C12), 31155–31166.
- Gouretski, V., & Koltermann, K. P. (2004). Woce global hydrographic climatology. *Berichte des BSH*, 35, 1–52.
- Graffino, G., Farneti, R., Kucharski, F., & Molteni, F. (2019). The effect of wind stress anomalies and location in driving pacific subtropical cells and tropical climate. *Journal of Climate*, 32(5), 1641–1660.
- Gray, J. S., Wu, R. S.-s., & Or, Y. Y. (2002). Effects of hypoxia and organic enrichment on the coastal marine environment. *Marine ecology progress series*, 238, 249–279.
- Griffies, S. M., Biastoch, A., Bärning, C., Bryan, F., Danabasoglu, G., Chassignet, E. P., ... Yin, J. (2009). Coordinated ocean-ice reference experiments (cores). *Ocean modelling*, 26(1-2), 1–46.
- Hahn, J., Brandt, P., Greatbatch, R. J., Krahmann, G., & Körtzinger, A. (2014). Oxygen variance and meridional oxygen supply in the tropical north east atlantic oxygen minimum zone. *Climate Dynamics*, 43, 2999–3024.
- Halpern, D., Knox, R. A., & Luther, D. S. (1988). Observations of 20-day period meridional current oscillations in the upper ocean along the pacific equator. *Journal of Physical Oceanography*, 18(11), 1514–1534.
- Harrison, C. S., Long, M. C., Lovenduski, N. S., & Moore, J. K. (2018). Mesoscale effects on carbon export: a global perspective. *Global Biogeochemical Cycles*, 32(4), 680–703.
- Holmes, R., McGregor, S., Santoso, A., & England, M. H. (2019). Contribution of tropical instability waves to enso irregularity. *Climate Dynamics*, 52(3-4), 1837–1855.
- Holmes, R., & Thomas, L. (2015). The modulation of equatorial turbulence by tropical instability waves in a regional ocean model. *Journal of Physical Oceanography*, 45(4), 1155–1173.
- Inoue, R., Lien, R.-C., & Moum, J. (2012). Modulation of equatorial turbulence by a tropical instability wave. *Journal of Geophysical Research: Oceans*, 117(C10).
- Inoue, R., Lien, R.-C., Moum, J. N., Perez, R. C., & Gregg, M. C. (2019). Variations of equatorial shear, stratification, and turbulence within a tropical instability wave cycle. *Journal of Geophysical Research: Oceans*, 124(3), 1858–1875.
- Ito, T., Minobe, S., Long, M. C., & Deutsch, C. (2017). Upper ocean o₂ trends: 1958–2015. *Geophysical Research Letters*, 44(9), 4214–4223.
- Johnson, G. C., & McPhaden, M. J. (1999). Interior pycnocline flow from the subtropical to the equatorial pacific ocean. *Journal of Physical Oceanography*, 29(12), 3073–3089.
- Johnson, G. C., Sloyan, B. M., Kessler, W. S., & McTaggart, K. E. (2002). Direct measurements of upper ocean currents and water properties across the tropical pacific during the 1990s. *Progress in Oceanography*, 52(1), 31–61.
- Karstensen, J., Stramma, L., & Visbeck, M. (2008). Oxygen minimum zones in the eastern tropical atlantic and pacific oceans. *Progress in Oceanography*, 77(4), 331–350.
- Keeling, R. F., & Garcia, H. E. (2002). The change in oceanic o₂ inventory associated with recent global warming. *Proceedings of the National Academy of Sciences*, 99(12), 7848–7853.

- Keeling, R. F., Körtzinger, A., & Gruber, N. (2010). Ocean deoxygenation in a warming world. *Annual review of marine science*, 2, 199–229.
- Kennan, S. C., & Flament, P. J. (2000). Observations of a tropical instability vortex. *Journal of Physical Oceanography*, 30(9), 2277–2301.
- Kessler, W. S. (2006). The circulation of the eastern tropical pacific: A review. *Progress in Oceanography*, 69(2-4), 181–217.
- Large, W. G., Danabasoglu, G., Doney, S. C., & McWilliams, J. C. (1997). Sensitivity to surface forcing and boundary layer mixing in a global ocean model: Annual-mean climatology. *Journal of Physical Oceanography*, 27(11), 2418–2447.
- Large, W. G., & Gent, P. R. (1999). Validation of vertical mixing in an equatorial ocean model using large eddy simulations and observations. *Journal of Physical Oceanography*, 29(3), 449–464.
- Large, W. G., McWilliams, J. C., & Doney, S. C. (1994). Oceanic vertical mixing: A review and a model with a nonlocal boundary layer parameterization. *Reviews of Geophysics*, 32(4), 363–403.
- Large, W. G., & Yeager, S. G. (2004). *Diurnal to decadal global forcing for ocean and sea-ice models: The data sets and flux climatologies*. National Center for Atmospheric Research Boulder.
- Lee, T., & Fukumori, I. (2003). Interannual-to-decadal variations of tropical–subtropical exchange in the pacific ocean: Boundary versus interior pycnocline transports. *Journal of Climate*, 16(24), 4022–4042.
- Lévy, M., Resplandy, L., Palter, J. B., Couespel, D., & Lachkar, Z. (2022). The crucial contribution of mixing to present and future ocean oxygen distribution. In *Ocean mixing* (pp. 329–344). Elsevier.
- Lien, R.-C., d’Asaro, E. A., & Menkes, C. E. (2008). Modulation of equatorial turbulence by tropical instability waves. *Geophysical Research Letters*, 35(24).
- Long, M. C., Lindsay, K., Peacock, S., Moore, J. K., & Doney, S. C. (2013). Twentieth-century oceanic carbon uptake and storage in cesm1 (bgc). *Journal of Climate*, 26(18), 6775–6800.
- Margolskee, A., Frenzel, H., Emerson, S., & Deutsch, C. (2019). Ventilation pathways for the north pacific oxygen deficient zone. *Global Biogeochemical Cycles*, 33(7), 875–890.
- McGillicuddy Jr, D., Anderson, L., Doney, S., & Maltrud, M. (2003). Eddy-driven sources and sinks of nutrients in the upper ocean: Results from a 0.1 resolution model of the north atlantic. *Global Biogeochemical Cycles*, 17(2).
- Moore, J. K., Lindsay, K., Doney, S. C., Long, M. C., & Misumi, K. (2013). Marine ecosystem dynamics and biogeochemical cycling in the community earth system model [cesm1 (bgc)]: Comparison of the 1990s with the 2090s under the rcp4. 5 and rcp8. 5 scenarios. *Journal of Climate*, 26(23), 9291–9312.
- Moum, J. (2021). Variations in ocean mixing from seconds to years. *Annual Review of Marine Science*, 13, 201–226.
- Moum, J., Lien, R.-C., Perlin, A., Nash, J., Gregg, M., & Wiles, P. (2009). Sea surface cooling at the equator by subsurface mixing in tropical instability waves. *Nature Geoscience*, 2(11), 761–765.
- Moum, J., Perlin, A., Nash, J. D., & McPhaden, M. J. (2013). Seasonal sea surface cooling in the equatorial pacific cold tongue controlled by ocean mixing. *Nature*, 500(7460), 64–67.
- Oschlies, A., Brandt, P., Stramma, L., & Schmidtko, S. (2018). Drivers and mechanisms of ocean deoxygenation. *Nature Geoscience*, 11(7), 467–473.
- Portela, E., Kolodziejczyk, N., Vic, C., & Thierry, V. (2020). Physical mechanisms driving oxygen subduction in the global ocean. *Geophysical Research Letters*, 47(17), e2020GL089040.
- Rohr, T., Harrison, C., Long, M. C., Gaube, P., & Doney, S. C. (2020). The simulated biological response to southern ocean eddies via biological rate

- modification and physical transport. *Global Biogeochemical Cycles*, 34(6), e2019GB006385.
- Ryan, J. P., Ueki, I., Chao, Y., Zhang, H., Polito, P. S., & Chavez, F. P. (2006). Western pacific modulation of large phytoplankton blooms in the central and eastern equatorial pacific. *Journal of Geophysical Research: Biogeosciences*, 111(G2).
- Schmidtko, S., Stramma, L., & Visbeck, M. (2017). Decline in global oceanic oxygen content during the past five decades. *Nature*, 542(7641), 335.
- Sen Gupta, A., Ganachaud, A., McGregor, S., Brown, J. N., & Muir, L. (2012). Drivers of the projected changes to the pacific ocean equatorial circulation. *Geophysical Research Letters*, 39(9).
- Smith, R., Jones, P., Briegleb, B., Bryan, F., Danabasoglu, G., Dennis, J., ... Hecht, M. (2010). The parallel ocean program (pop) reference manual: ocean component of the community climate system model (ccsm) and community earth system model (cesm). *Rep. LAUR-01853*, 141, 1–140.
- Smyth, W., & Moum, J. (2013). Marginal instability and deep cycle turbulence in the eastern equatorial pacific ocean. *Geophysical Research Letters*, 40(23), 6181–6185.
- Song, H., Long, M. C., Gaube, P., Frenger, I., Marshall, J., & McGillicuddy Jr, D. J. (2018). Seasonal variation in the correlation between anomalies of sea level and chlorophyll in the antarctic circumpolar current. *Geophysical Research Letters*, 45(10), 5011–5019.
- Stramma, L., Johnson, G. C., Firing, E., & Schmidtko, S. (2010). Eastern pacific oxygen minimum zones: Supply paths and multidecadal changes. *Journal of Geophysical Research: Oceans*, 115(C9).
- Stramma, L., Prince, E. D., Schmidtko, S., Luo, J., Hoolihan, J. P., Visbeck, M., ... Körtzinger, A. (2012). Expansion of oxygen minimum zones may reduce available habitat for tropical pelagic fishes. *Nature Climate Change*, 2(1), 33.
- Strutton, P. G., Palacz, A. P., Dugdale, R. C., Chai, F., Marchi, A., Parker, A. E., ... Wilkerson, F. P. (2011). The impact of equatorial pacific tropical instability waves on hydrography and nutrients: 2004–2005. *Deep Sea Research Part II: Topical Studies in Oceanography*, 58(3–4), 284–295.
- Strutton, P. G., Ryan, J. P., & Chavez, F. P. (2001). Enhanced chlorophyll associated with tropical instability waves in the equatorial pacific. *Geophysical Research Letters*, 28(10), 2005–2008.
- Sverdrup, H. (1938). On the explanation of the oxygen minima and maxima in the oceans. *ICES Journal of Marine Science*, 13(2), 163–172.
- Tanaka, Y., Hibiya, T., & Sasaki, H. (2015). Downward lee wave radiation from tropical instability waves in the central equatorial pacific ocean: A possible energy pathway to turbulent mixing. *Journal of Geophysical Research: Oceans*, 120(11), 7137–7149.
- Tian, F., Zhang, R.-H., & Wang, X. (2018). A coupled ocean physics-biology modeling study on tropical instability wave-induced chlorophyll impacts in the pacific. *Journal of Geophysical Research: Oceans*, 123(8), 5160–5179.
- Ubelmann, C., & Fu, L.-L. (2011). Vorticity structures in the tropical pacific from a numerical simulation. *Journal of physical oceanography*, 41(8), 1455–1464.
- Vaquer-Sunyer, R., & Duarte, C. M. (2008). Thresholds of hypoxia for marine biodiversity. *Proceedings of the National Academy of Sciences*, 105(40), 15452–15457.
- Vecchi, G. A., Soden, B. J., Wittenberg, A. T., Held, I. M., Leetmaa, A., & Harrison, M. J. (2006). Weakening of tropical pacific atmospheric circulation due to anthropogenic forcing. *Nature*, 441(7089), 73–76.
- Vichi, M., Masina, S., & Nencioli, F. (2008). A process-oriented model study of equatorial pacific phytoplankton: the role of iron supply and tropical instability waves. *Progress in Oceanography*, 78(2), 147–162.

- 729 Whitt, D., Cherian, D., Holmes, R., Bachman, S., Lien, R.-C., Large, W., & Moum,
730 J. (2022). Simulation and scaling of the turbulent vertical heat transport and
731 deep-cycle turbulence across the equatorial pacific cold tongue. *Journal of*
732 *Physical Oceanography*, 52(5), 981–1014.
- 733 Willett, C. S., Leben, R. R., & Lavín, M. F. (2006). Eddies and tropical instabil-
734 ity waves in the eastern tropical pacific: A review. *Progress in Oceanography*,
735 69(2-4), 218–238.
- 736 Wyrski, K. (1962). The oxygen minima in relation to ocean circulation. In *Deep sea*
737 *research and oceanographic abstracts* (Vol. 9, pp. 11–23).
- 738 Ying, J., Collins, M., Cai, W., Timmermann, A., Huang, P., Chen, D., & Stein, K.
739 (2022). Emergence of climate change in the tropical pacific. *Nature Climate*
740 *Change*, 12(4), 356–364.
- 741 Zaron, E. D., & Moum, J. N. (2009). A new look at richardson number mixing
742 schemes for equatorial ocean modeling. *Journal of physical oceanography*,
743 39(10), 2652–2664.

Supporting Information for

Eddy-Mediated Mixing of Oxygen in the Equatorial Pacific

Yassir A. Eddebbar¹, Daniel B. Whitt², Ariane Verdy¹, Matthew R. Mazloff¹,
Aneesh C. Subramanian³, Matthew C. Long⁴

¹Scripps Institution of Oceanography, University of California San Diego, La Jolla, CA

²Ames Research Center, NASA, Moffett Field, CA

³Atmospheric and Oceanic Sciences, Colorado University, Boulder, CO

⁴National Center for Atmospheric Research, Boulder, CO

Contents of this file

Figures S1 to S4

Introduction

This document includes supporting figures S1 through S4.

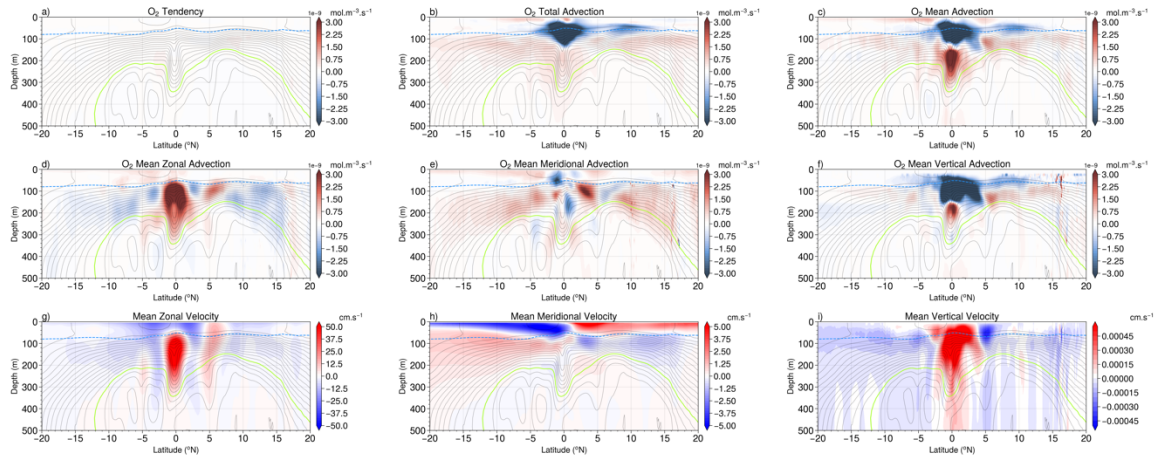


Figure S1. a) O₂ tendency, b) total advection, and c) mean advection terms averaged over 80°W-160°W in CESM. The decomposition of the mean advection term is shown for d) zonal, e) meridional, f) vertical advection, along with climatological mean g) zonal, h) meridional, and i) vertical velocities in CESM averaged over 80°W-160°W. Positive velocities in g-i) denote eastward, northward, and downward flow, respectively.

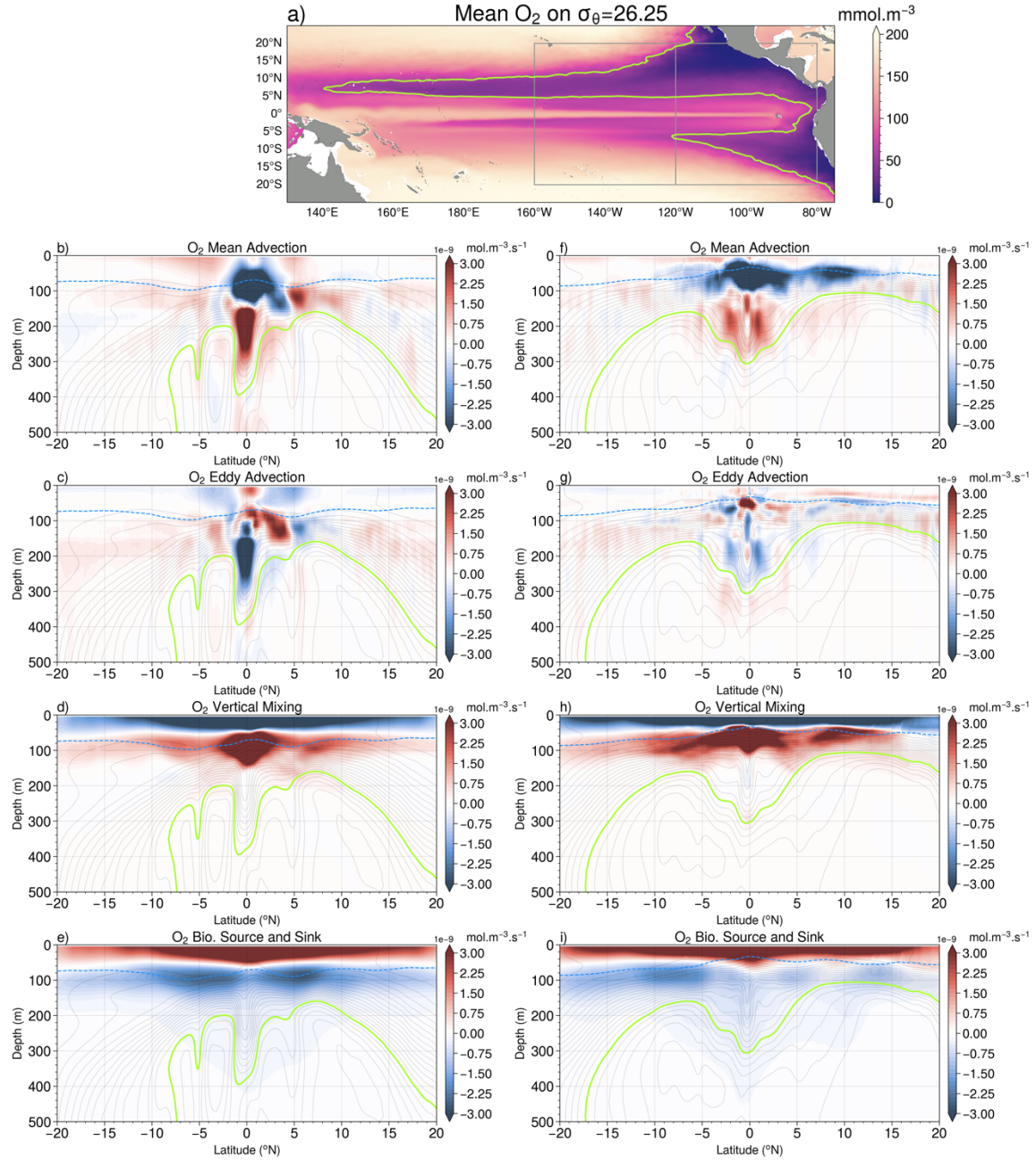


Figure S2. Mean O_2 budget decomposition averaged over the central (left panels) and eastern (right panels) equatorial Pacific in CESM, including a) mean O_2 concentrations on the 26.25 isopycnal, and contributions of b) mean advection, c) eddy advection, d) vertical mixing, and e) biogeochemical (production - consumption) sources and sinks for the central (160°W-120°W) equatorial Pacific. Panels f-i) same as b-e) but for the eastern (120°W-80°W) equatorial Pacific. Grey boxes in a) outline these two regions.

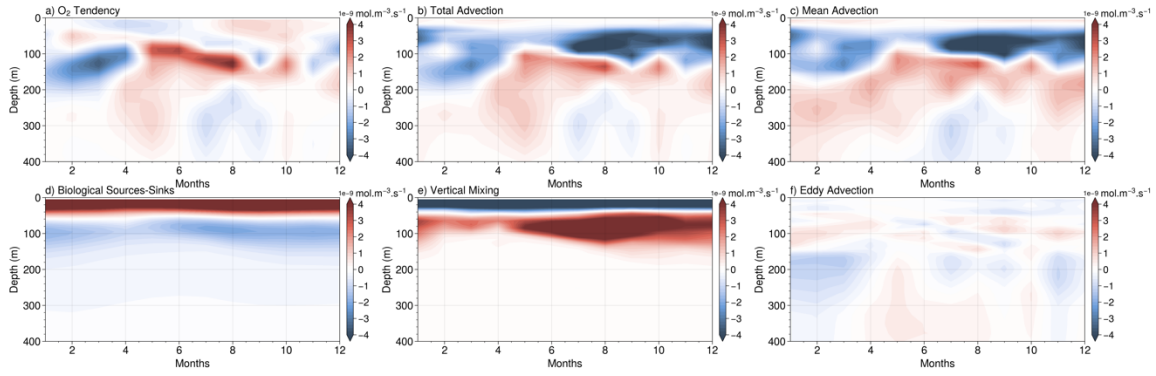


Figure S3. Seasonal O_2 budget balance averaged over the eastern and central equatorial Pacific ($7^{\circ}S$ - $7^{\circ}N$ and $80^{\circ}W$ - $160^{\circ}W$) in CESM, including a) O_2 tendency, b) total advection, c) mean advection, d) biological sources and sinks, e) vertical mixing, and f) eddy advection.

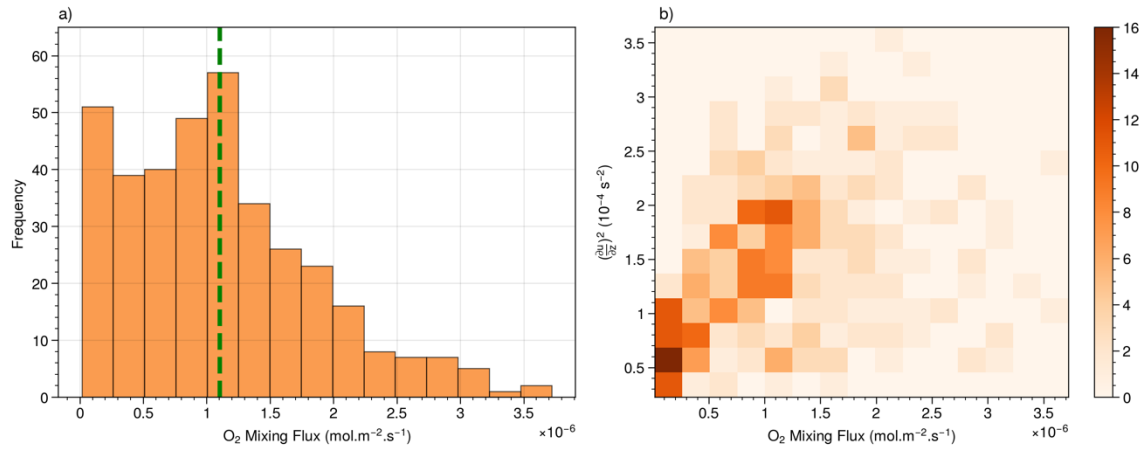


Figure S4. a) Histogram of the vertical turbulent mixing flux of O_2 at 0° $140^{\circ}W$ for the 5 year CESM simulation, with the climatological mean value outlined by the green dashed vertical line. b) 2d histogram of the vertical turbulent mixing flux of O_2 vs the squared vertical shear of zonal velocity at 0° $140^{\circ}W$ averaged vertically over the low-Ri layer. The vertical O_2 mixing flux term shown in a) and b) represent the depth-maximum in the downward local turbulent mixing flux of O_2 .